

<https://doi.org/10.1038/s41545-024-00319-4>

Manufacturing supported loose-nanofiltration polymeric membranes with eco-friendly solvents on an R2R System

Check for updates

David Lu^{1,3}, Kwangjun Jung^{2,3}, Ju Young Shim², Tequila A. L. Harris² & Isabel C. Escobar¹

In this study, loose nanofiltration membranes made of polysulfone dissolved in co-solvents PolarClean and gamma-Valerolactone were prepared via slot die coating (SDC) on a roll-to-roll (R2R) system by directly coating them onto a support layer or free standing. A solution flow rate of 20 mL/min, substrate speed of 17.1 mm/s, and coating gap of 0.1 mm resulted in the formation of membranes without structural defects. Pre-wetting the support layer with dope solution minimized shrinkage of membrane layer thickness and improved interfacial adhesion. Membrane samples produced using SDC exhibited properties and performance consistent with bench-scale doctor blade extruded samples; pre-wetted and uncompressed samples (SDC-3) exhibited the highest rejection of bovine serum albumin ($99.20\% \pm 1.31\%$) and along with adequate mean permeability during filtration (70.5 ± 8.33 LMH/bar). This study shows that combining sustainable materials development with SDC provides a holistic approach to membrane separations to bridge materials discovery and membrane formation.

In comparison to traditional separation technologies, membranes have become an advantageous option due to generally fewer manufacturing costs, lower energy requirements, and operating flexibility while still offering high permeability and selectivity^{1–3}. With an abundant range of commercially available polymers, solvents, and additive materials, polymeric membranes can be tailored for specific properties and applications. A myriad of industrial separations, including water treatment, bio-separations, gas separations, and electrodialysis, can be performed using polymeric membranes⁴. New materials and chemistries are the focus of much academic research to address difficult separations, control fouling and develop multi-functional membranes. In particular, there has been significant research in developing polymeric membranes imbued with the intrinsic properties and advantages of both traditional ultrafiltration (UF) and nanofiltration (NF) membranes to achieve high solute rejection and permeability. Loose NF membranes (LNF) fall in between these two membrane classifications and are capable of removing organic macromolecules with a significantly higher permeability than tight NF membranes and a higher selectivity than other UF membranes^{5,6}. As such, there is a strong demand for developing manufacturing processes to produce these membranes at the commercial scale. However, aligning the manufacturing processes with the two modern principles of scalability and eco-manufacturing poses a major hurdle in optimizing commercial-scale polymeric membrane fabrication.

Currently, MF, UF, LNF, and tight NF polymeric membranes are commonly produced using phase inversion methods⁷. Nonsolvent-induced phase separation (NIPS) is considered the dominant phase separation technique, in which a dope solution is cast onto a solid substrate and immersed in a nonsolvent coagulation bath, most commonly water^{7,8}. Solvent from the film exchanges with the nonsolvent, causing the film to form a solid, polymer-rich membrane matrix with polymer-poor phase areas that become the pores; the end-product is an asymmetric membrane with a dense selective layer and a porous sublayer for mechanical stability^{9–12}.

Bench-scale polymeric membrane fabrication via NIPS has been extensively studied and is generally conducted using doctor blade extrusion (DBE), spin coating, and dip coating¹³. In particular, DBE is one of the most common methods to develop bench-scale membranes but is not considered ideal for integration into an R2R system to produce membranes with consistent functionality^{13,14}. Alternatively, slot die coating (SDC) is a method commonly used for thin film manufacturing that overcomes this drawback of DBE. In SDC, a slot die deposits a fluid onto a moving substrate to form the film^{15,16}. SDC offers greater flexibility in film thickness and can be integrated into a roll-to-roll (R2R) system for continuous casting⁷. SDC is among the most widely used manufacturing processes for thin film across many applications, however, there are limited studies of R2R manufacturing of membranes with SDC for clean

¹Department of Chemical and Materials Engineering, University of Kentucky, Lexington, KY 40506, USA. ²George W. Woodruff School of Mechanical Engineering, Georgia Institute of Technology, Atlanta, GA 30332, USA. ³These authors contributed equally: David Lu, Kwangjun Jung. e-mail: tharris3@gatech.edu; Isabel.Escobar@uky.edu

water applications^{5,11,12}. A general illustration of the coating process for SDC as compared to DBE is found in Fig. 1.

As reported in several studies on polymeric membrane scale-up using SDC, a careful balance of parameters (e.g., substrate speed, solution flow rate) is crucial in forming uniform membranes^{14,17}; the range of adequate casting parameters for uniform membrane formation can be visualized as a casting or coating window^{14,18}, where the difference between casting and coating is whether the dried film is removed from or remains on the substrate, respectively. The coating parameters are dependent on the substrate and dope solution properties, including the contact angles, surface tension, and viscosity since they can affect the substrate speed and flow behavior^{16,18,19}. Thus, a thorough analysis of the dope solution is the first step in developing a SDC method for polymeric membrane fabrication.

A common feature of polymeric membranes is the inclusion of a support layer acting as a substrate for the porous and selective layers. Different materials, including woven and nonwoven polyethylene terephthalate (PET) and polyester films, have been studied as a support layer for polymeric membranes²⁰. While the main advantage of a support layer is increased mechanical integrity, the support layer may also result in differences in the membrane morphology and filtration characteristics. Lohokare et al.²⁰ reported that casting a polyacrylonitrile UF membrane on Hollytex[®] nonwoven polyester fabric generally resulted in higher water flux, protein rejection, membrane forming capacity, and resistance to compaction than membranes cast onto a woven fabric layer. Oh et al.²¹ found that the non-woven support layer influenced the internal structure of the membrane; namely, a PET support layer resisted solvent/nonsolvent exchange and contributed to the formation of sponge-like pore structures associated with slower mixing/de-mixing. Of the available types of support layer materials, nonwoven PET fabrics are of notable interest due to their high permeability and tensile strength, which aid the filtration performance and enhance the membrane durability. Moreover, the high melting point of PET enables it to serve as a durable support layer for high temperature filtration applications, including NF filtration at temperatures up to 65 °C²². Hollytex[®] 3265 nonwoven PET fabric was selected as the support for this study as others have found enhanced water permeability due to increased pore formation^{20,23}. Notable properties of Hollytex[®] 3265 include a reported air permeability of 20 cfm, cross-directional tensile strength of 11.4 kg/m² (21 lbs/yd²), machine-direction tensile strength of 11.6 kg/cm (65 lbs/in), and water holding capacity of 28.26 wt %²⁰.

During the membrane fabrication process, the dope solution is generally cast directly onto the support layer material prior to immersion in a

nonsolvent bath. However, translating a direct coating method onto a SDC setup has yet to be demonstrated, which introduces the additional challenge of a substrate being placed over the traditional glass platen. Furthermore, analyses of the dope solution mixing kinetics in the presence of a support layer, the membrane-support layer interface, and the relationship between the support layer and membrane properties in scale-up studies remain largely unstudied.

Separately, eco-manufacturing has become a crucial manufacturing principle due to concerns about climate change impacts and environmental degradation associated with industrial manufacturing. The current industrial manufacturing sector contributes to 15% of global energy consumption and 35–40% of global material consumption, resulting in a push for identifying opportunities to reduce the energy, material, and fossil fuel footprints of manufacturing processes²⁴. In particular, two methods of eco-manufacturing that drive industrial sustainability are the reduction of waste and the incorporation of eco-friendly materials, both of which can be implemented in polymeric membrane manufacturing²⁴.

One of the main drawbacks of NIPS and other phase inversion methods is the frequent use of hazardous and fossil fuel-derived solvents in preparing the dope solution. Traditionally used solvents, including N-methyl-2-pyrrolidone (NMP), dimethylformamide (DMF) and dimethylacetamide (DMAc), pose hazards to human health (e.g., toxic, irritant, and carcinogenic properties) and the environment (e.g., flammable, toxic to aquatic life), elevating the risk of NIPS^{7,25}. Moreover, the petroleum-derived nature of these solvents increases the carbon footprint of the manufacturing process. Due to recent regulations on solvent use, there is now an emphasis on using eco-friendly solvents in polymeric membrane fabrication; along with mitigating safety hazards associated with the manufacturing process, the inclusion of eco-friendly solvents removes the costly and energy-intensive step of removing toxic solvents from the fabrication wastewater.

Recent advances in eco-friendly solvent development have resulted in the emergence of “green” dipolar aprotic candidates, including Cyrene, MeSesamol, and dimethyl isosorbide^{26–29}. Two notable eco-friendly solvents that meet these characteristics and are commercially available are methyl 5-(dimethylamino)-2-methyl-5-oxopentanoate (Rhodiasolv[®] PolarClean) and gamma-valerolactone (GVL). PolarClean is the chemical valorization product of methylglutarodinitrile (MDN), which itself is a solvent and a by-product of nylon 6,6 fabrication^{30–32}. The high miscibility and solubility of PolarClean in water make it a suitable alternative for traditional solvents, along with being reported as a non-toxic and biodegradable solvent^{31,33,34}. Moreover, the mass production of Nylon-6,6 and, subsequently, MDN

Fig. 1 | Schematic visualization of the doctor blade extrusion and slot die coating methods for polymeric membrane preparation.

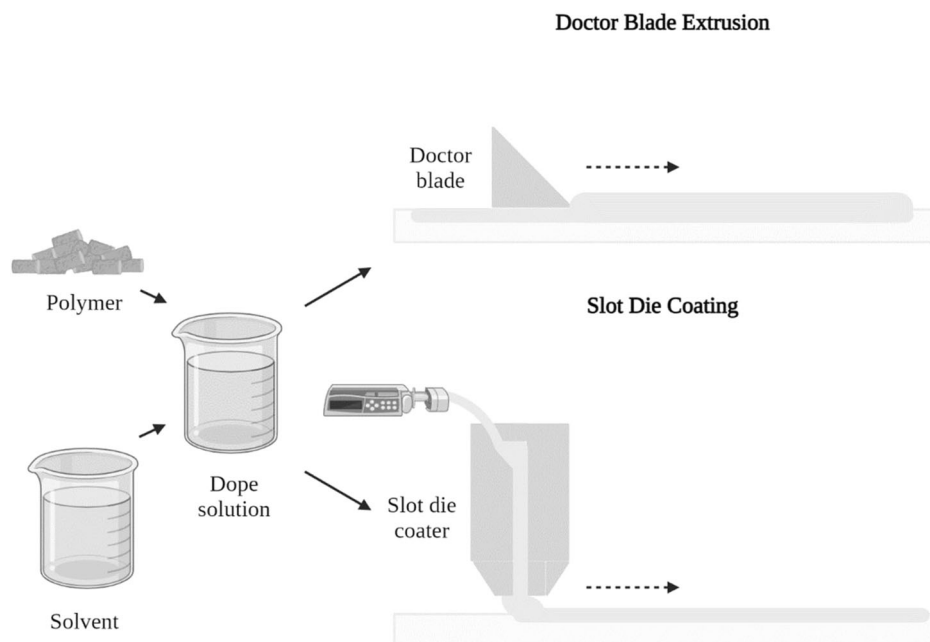
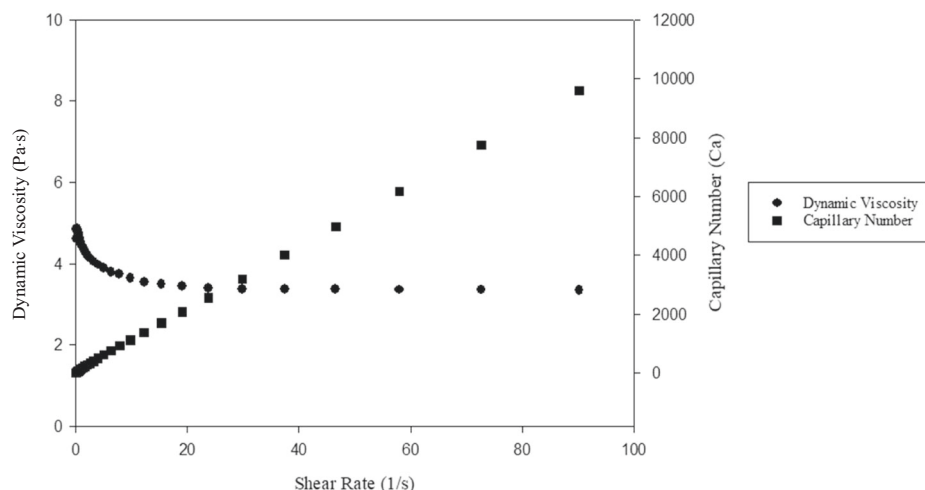


Fig. 2 | Dynamic viscosity and capillary number of the PSf-PolarClean-GVL dope solution from a shear rate of 0–90 s⁻¹. Viscosity data was first reported in Lu et al.⁴².



translates to large-scale availability and production of PolarClean³⁵. GVL is a cyclic ester derived from lignocellulosic biomass processing; it is another alternative solvent for NIPS due to its water solubility, non-toxicity, and biodegradability^{7,36}. As such, GVL has been used in a multitude of applications (e.g., lignin depolymerization, electrochemistry, solid phase peptide synthesis) as a reaction solvent^{37–39}. The individual use of PolarClean and GVL as solvents for polymeric membranes has been investigated, though studies on using the two solvents in combination have touted more favorable results^{11,14,25,30,33,34}. Polysulfone (PSf) membranes prepared using a 3:1 ratio of PolarClean-GVL have reported similar water permeability and bovine serum albumin (BSA) rejection compared to PSf membranes prepared using the traditional solvents DMAc and NMP²⁵. Additionally, the use of both solvents results in the formation of PSf membranes that are more durable than counterparts prepared using solely PolarClean or GVL²⁵.

Although recent studies have investigated methods for including support layers and eco-friendly solvents in bench-scale polymeric membranes, the next step of scale-up and direct coating onto a support layer using SDC on a R2R system, remains largely unstudied. Dong et al.¹⁴ reported successful fabrication of PSf-PolarClean-GVL UF flat sheet membranes using a SDC setup on a R2R system, in which the membranes exhibited similar surface roughness, flux, and selectivity to membranes prepared using the DBE method. Beyond these findings, analyses of the relationship between the dope solution properties, coating parameters, and film defect formation would further clarify the application of SDC for polymeric membrane fabrication. Additionally, the incorporation of a support layer would introduce a porous substrate to study these mechanisms, which have previously only been studied on a glass substrate¹⁴.

The goal of this study is to demonstrate the formation of loose-NF flat sheet membranes via slot die coating integrated into a R2R system, whether cast or coated onto a support layer and how the dope solution properties influence the and fabrication and membrane formation processes. Properties of an eco-friendly PSf-PolarClean-GVL dope solution were evaluated to determine the casting window for the SDC. PSf was selected as the polymer due to its prominent use in NF and UF polymeric membranes, strong thermal and chemical resistance properties, and low environmental impact^{40,41}. Membranes manufactured via SDC were compared with membrane samples fabricated via DBE to demonstrate the translation of the membrane properties and filtration capabilities during scale-up. For both fabrication methods, membranes were coated onto the support layer using different configurations to investigate the interface properties and changes in membrane performance.

Results

Properties of the Dope Solution

The dynamic viscosity of the PSf-PolarClean-GVL dope solution, which was first reported in Lu et al.⁴², is shown in Fig. 2. At the onset, the viscosity was

approximately 4.85 Pa·s before decreasing and stabilizing at approximately 3.39 Pa·s once the shear rate reached 30 s⁻¹. The shear-thinning behavior observed in this initial range suggested the occurrence of polymer chain disentanglement, which was complete once the shear rate reached 30 s⁻¹^{43,44}. Moreover, this shear-thinning behavior is consistent with conventional polymer solutions^{45,46}. The dope solution was considered suitable for DBE since dynamic viscosity was generally uniform at higher shear rates, which would result in a cast/coated film with relatively uniform thickness and properties. Using SDC as a membrane fabrication method was also determined to be feasible since the dynamic viscosity was within range of the reported operating limits of SDC (1 m Pa·s ≤ ν ≤ several kPa·s)^{14,47}. Since the same dope solution was used to prepare all membrane samples, viscosity was set as a constant parameter.

Viscosity is a crucial parameter that influences film formation when SDC is used; namely, the flow behavior and formation of defects on the film can be dependent on the magnitude of viscous forces¹⁸. The capillary number, simply defined as the ratio of viscous forces to surface tension forces being acted upon a fluid, was calculated at each shear rate interval to characterize the dope solution viscosity and is also shown in Fig. 2¹⁶. Across all shear rates, the capillary number was significantly larger than 0.1, classifying the dope solution as a high-viscosity solution and indicating that viscous forces would be the dominant force experienced during substrate motion, particularly at high shear rates⁴⁸. Moreover, as a high-viscosity solution with some shear-thinning behavior exhibited, relatively low processing speeds would be required to produce a uniform membrane sheet¹⁶.

The mean surface tension for the dope solution was measured to be 31.5 ± 1.3 mN/m. Similar to viscosity, the surface tension of the sample was within the reported operating limits for this application (25 mN/m ≤ γ ≤ 500 mN/m)¹⁸. The surface tension measurement was also used to calculate the penetration length of the solution through porous media using Eq. 2. The calculated penetration length was 0.15 mm. Given that the thickness of the support layer is 0.12 mm, this observation suggests complete penetration of the solution through the support layer. Thus, an initial wetting treatment for the support layer was deemed necessary to minimize solution penetration. Wetting of the support layer using a solvent has been studied, though the presence of additional solvent during the fabrication process may dilute the dope solution and alter the membrane properties⁴⁹; thus, the dope solution was selected as the wetting agent in this study. The various configurations of the membrane and support layer visualized in Table 1 were explored to minimize the penetration of the dope solution through the support layer.

The contact angle value indicates relatively favorable wettability of a solution on the substrate surface⁵⁰. In SDC, the wettability of the slot coater material can determine the magnitude of capillary flow of the fluid through the device. A higher contact angle for the slot die versus the substrate is preferred to aid favorable flow through the slot coater and reduced viscous

forces. The mean contact angles for the dope solution on the various substrates studied are shown in Table 2. The mean contact angle on glass was $20.7^\circ \pm 1.7^\circ$, indicating favorable wettability. Two metallic plates, aluminum and stainless steel, were selected as candidates for the slot coater material. Mean contact angle measurements for the aluminum and stainless-steel surfaces were relatively similar at $28.8^\circ \pm 1.9^\circ$ and $31.5^\circ \pm 1.8^\circ$, respectively. Since stainless steel exhibited the highest mean contact angle, a stainless-steel slot die coater was selected to be used in the SDC system.

Membrane formation using SDC

Determining the operating limits of materials in the slot die coating process is crucial, as it enables the fabrication of membranes with the desired thickness without any defects by tuning the coating parameters within the identified stable coating region¹⁸. Through the well-established correlation between flow rate and substrate speed in this system¹⁸, a partial coating window for the PSf-PolarClean-GVL dope solution cast on a glass plate was determined. For these experiments, the flow rate was set within the range of 3.5–90 ml/min and the substrate speed ranged from 5.4 to 40.2 mm/s and the coating gap was set as 0.1 mm. Supplementary Fig. 1a illustrates a membrane sample formed at the upper boundary and Supplementary Fig. 1b illustrates the process at the lower boundary of the parameter ranges, as well as the resulting defect formations. Limitations of the coating parameters was derived by the acoustic noise in the coating system at higher coating parameter. As one parameter was altered and the other remained constant, either air entrainment or dripping phenomena were observed, to construct the upper and lower boundaries of the partial coating window for processing the PSf-PolarClean-GVL dope solution on a glass plate, as shown in Fig. 3a. Visual representation of coating instability leading to air entrainment and dripping phenomena is captured in Fig. 3b, c. Uniform membranes with a desired thickness reside within the partial coating window. Near the intersection of the upper and lower boundaries, fluid flow instability caused by the casting parameters led to membranes with defects, which are (b) shown in Supplementary Fig. 1a, b.

A series of experiments were carried out to fabricate the defect-free membranes through optimal coating parameters based on the partial casting window. Despite avoiding coating-related defects, samples initially exhibited surface wrinkling as shown in Supplementary Fig. 2. Similar phenomenon was observed by Blanco et al.⁵¹ and proposed potential causes for this observation. The surface layer becomes progressively harder as the coagulation process proceeds and the membrane's surface layer hardens due to the solvent extraction into the non-solvent bath. Concurrently, the underlying substrate remains in a fluid state until the entire membrane solidifies. This differential setting process results in the development of compressive strain in the surface layer, causing random deflections or wrinkles⁵¹. To mitigate wrinkling, casting the membrane on a hard, rigid substrate is beneficial. The rigid substrate supports the aqueous part of the dope solution to withstand the compressive stress encountered during the solidification of the surface layer in the NIPS process. However, for a thicker film, the bulk of fluid part of the dope solution beneath the surface layer lacks the mechanical strength to resist the imposed stresses, resulting in the generation of wrinkles. This observation led to implementing a set of experiments to tune the casting parameters to eliminate the wrinkle formation during NIPS process as well as producing the membranes with desired thickness ranged between 100 μm and 200 μm . As reported in Dong et al.⁷, manipulating the coating thickness alters the phase inversion process and the resulting membrane morphology. Membranes cast with greater thickness have exhibited macrovoids and finger-like pore structures, whereas decreasing the thickness led to the formation of denser, sponge-like pore structures akin to those found in this study^{52–55}. Thus, using a low casting thickness between 150 and 300 μm results in the formation of membranes with a compact pore structure, reduced shrinkage after casting, and efficient filtration performance^{25,53,56}. Additionally, Lu et al.⁴² investigated how the doctor blade casting conditions affected the membrane thickness for PSf-PolarClean-GVL membranes, particularly the effect of altering the evaporation time step between casting and film immersion in

the nonsolvent bath. Setting an evaporation time of around 30 s resulted in the thickening of the selective skin layer, which improved BSA rejection without a significant decline in permeability. This principle was applied in this study by setting an evaporation time of 20 s.

In the slot die coating process, there are three distinct coating regions (I, II, and III). The region depends on the fluid properties, die geometry, and flow parameters^{57,58}. As the capillary number increases in slot die coating process, the capillary force becomes negligible, while viscous, surface tension, and inertial force become dominant in creating the stable coating bead [15]. Experimental results from slot die coating processes, using Newtonian or approximately Newtonian solutions where the viscous force is dominant, showed that the minimum wet thickness with a vacuum pressure of 0, t_0 , ranged between $0.5 h_d$ and $0.7 h_d$, where h_d refers to the downstream coating gap⁵⁷. The system presented in this study had no vacuum pressure applied and the measured values were similar: the wet thickness at the lower boundary of the coating window was about 0.05 mm at the downstream coating gap of 0.1 mm. This observation suggests that the viscous force is dominant, thus the coating gap was increased from 0.1 mm to 0.2 mm to meet the target thickness. According to the experimental results by Chang et al.⁵⁹ and Chang et al.⁶⁰, the coating gap has a negligible effect on the coating window in the region where viscous force is dominant. Therefore, the partial coating window found in Fig. 3a was used to determine coating parameters to create uniform membranes.

To this end, a series of preliminary experiments were performed to measure the ratio of wet-to-dry thickness of the membranes fabricated at various casting parameters within the stable coating region. The wet and dry film thickness in these experiments were measured and the wet-to-dry film ratio was determined to be $57.7 \pm 9.5\%$. Based on the partial coating window shown in Fig. 3a and wet-to-dry film ratio, the substrate speed was held constant at 17.1 mm/s and flow rate was varied to analyze the resulting membranes. The substrate speed was chosen in such a way that the system minimized any acoustic noise involved during the fabrication process and ensured the production of membranes in the most scaled manner. At a given substrate speed of 17.1 mm/s, when the flow rate was lower than 20 mL/min, the wet thickness was lower than 0.11 mm and ribbing was often observed during the NIPS process. The presence of this defect could be due to the nonuniformity of the fluid coating on the glass platen with viscous forces overcoming the capillary pressure during the casting process. As a result of this observation, the flow rate needed to be increased. When the flow rate was increased to 25 mL/min, the wet thickness was approximately 0.23 mm and despite the uniform wet surface, wrinkle formation was observed on the surface of the membrane during NIPS process. These observations indicated the need to lower the wet thickness to less than 0.23 mm, since thicker films are more prone to wrinkle formation during the NIPS process. Additionally, a reduction in the flow rate is needed to produce uniform films. Hence, a flow rate of 20 mL/min and substrate speed of 17.1 mm/s were selected as a set of casting parameters that would not result in defects. To ensure that the process reached a steady state, multiple glass plates were continuously fed into the system. The cast membranes were then submerged into a DI water bath to undergo the NIPS process coagulation. As a result, uniform membranes with mean wet film thickness of 0.156 mm and mean dried film thickness of 0.09 mm were successfully fabricated, as shown in Supplementary Fig. 3.

Based on the calculation from Washburn equation indicating the complete penetration of membrane through porous support layer, pre-coating processes were implemented to prevent the complete penetration of the dope solution and formation of a membrane thinner than designed. Dope solution penetration has been reportedly observed when casted onto a Hollytex 3265 support layer, which may be attributed to the attraction of polar groups found in the solvent and PET film surface. Namely, the amide group found in PolarClean, as well as the ester groups in PolarClean, GVL, and the PET film, contribute to the polarity of the dope solution and support layer and promote attraction between the two layers²⁵. As such, further characterization of SDC-2 was not conducted to focus on samples with a pre-coating step. For the pre-coating process, the support layers were

Table 1 | Fabrication process steps and filtration experiment configurations for each membrane sample prepared using doctor blade extrusion (DBE) and slot die coating (SDC) (all samples were prepared using a dope solution concentration of 17 wt% polymer, 83 wt% solvent, and at room temperature (21.1 °C ± 1.9 °C))

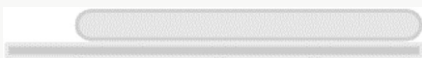
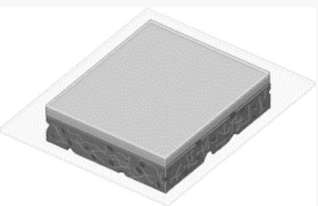

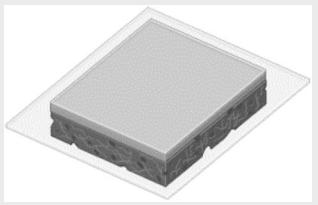

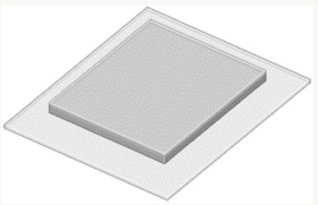

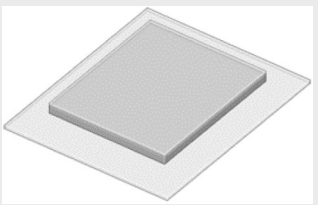
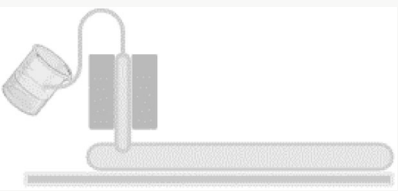
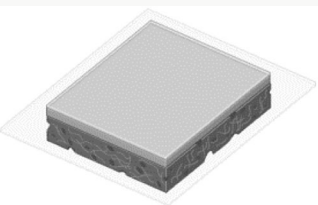
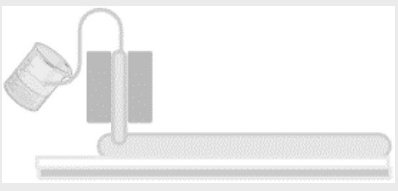
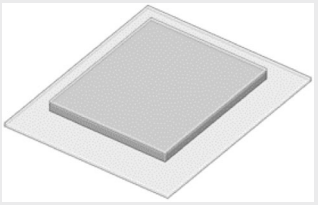
Doctor Blade Extrusion (DBE)		
Sample ID	Fabrication Process	Filtration Configuration
DBE-1	Solution coated onto glass plate with 0.2 mm coating gap, 200 cm/min casting speed 	Filter paper placed underneath membrane 
DBE-2	Solution coated onto glass plate with 0.2 mm coating gap, 200 cm/min casting speed 	Support layer placed underneath membrane 
DBE-3	Solution coated onto support layer sheet with 0.2 mm coating gap, 200 cm/min coating speed 	Support layer connected to membrane 
DBE-4	Solution coated onto support layer sheet with 0.05 mm coating gap; solution coated on top of previously coated film with 0.2 mm coating gap, 200 cm/min casting speed 	Support layer connected to membrane 
Slot Die Coating (SDC)		
Sample ID	Fabrication Process	Filtration Configuration
SDC-1	Solution coated onto glass platen with 0.2 mm coating gap, 3.5–90 mL/min flow rate, 5.4–40.2 mm/s substrate speed 	Filter paper placed underneath membrane 
SDC-2	Solution coated onto support layer sheet with 0.2 mm coating gap, 3.5–90 mL/min flow rate, 5.4–40.2 mm/s substrate speed 	Support layer connected to membrane 

Table 1 (continued) | Fabrication process steps and filtration experiment configurations for each membrane sample prepared using doctor blade extrusion (DBE) and slot die coating (SDC) (all samples were prepared using a dope solution concentration of 17 wt% polymer, 83 wt% solvent, and at room temperature (21.1 °C ± 1.9 °C))

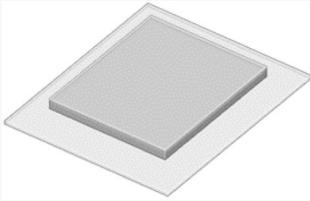
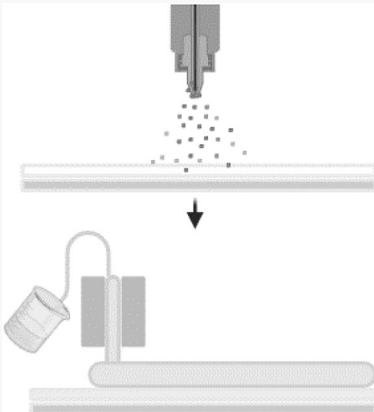
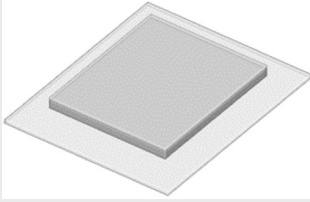
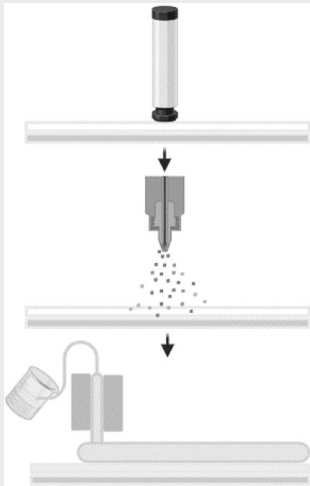
Doctor Blade Extrusion (DBE)		
Sample ID	Fabrication Process	Filtration Configuration
SDC-3	Support layer sheet spray-coated onto support layer sheet for 3 min at 5.52 psi; solution coated onto support layer sheet with 0.2 mm coating gap, 3.5–90 mL/min flow rate, 5.4–40.2 mm/s substrate speed	Support layer connected to membrane 
		
SDC-4	Support layer sheet compressed using rolling pin; support layer sheet spray-coated onto support layer sheet for 3 min at 5.52 psi; solution coated onto support layer sheet with 0.2 mm coating gap, 3.5–90 mL/min flow rate, 5.4–40.2 mm/s substrate speed	Support layer connected to membrane 
		

Table 2 | Contact Angle Measurements of PSf-PolarClean-GVL Dope Solutions on Glass, Aluminum, and Stainless-Steel Surfaces

Substrate	Contact angle (°)
Glass	20.7 ± 1.7
Aluminum	28.8 ± 1.9
Stainless Steel	31.5 ± 1.8

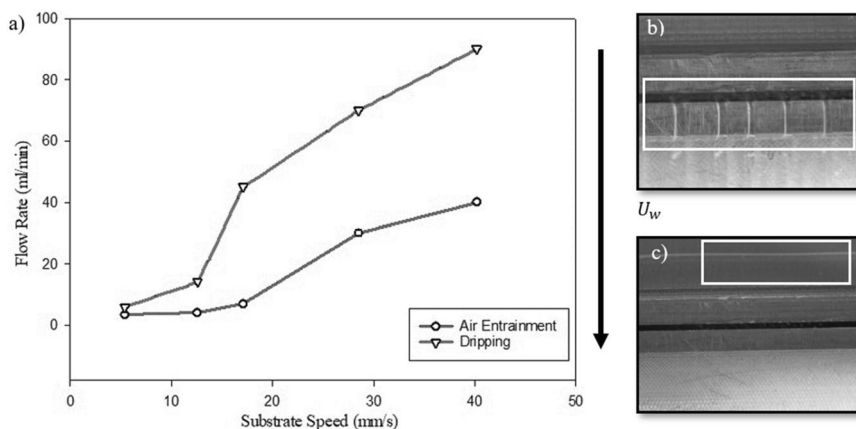
pre-spray-coated with PSf-PolarClean-GVL at 5.52 bar (80 psi) and either left uncompressed (SDC-3) or compressed (SDC-4). The support layer was compressed with rolling pins, resulting in a 0.01 mm decrease in thickness of the support layer. Continuous processing of three glass plates, two with support layers taped flat on all four sides on the glass plate, ensured that the system achieved a steady state. Accounting the calculated penetration length (0.15 mm) and adopting the same casting parameters (dope flow rate of 20 mL/min and substrate speed of 17.1 mm/s), PSf-PolarClean-GVL was cast onto the pre-conditioned support layers. The cast membrane was then

submerged in DI water bath to undergo phase inversion. Uncompressed and compressed coated support layers of uniform membranes with thicknesses of 0.15 mm were obtained. Surface images of the three SDC membrane samples fabricated on the support layer are shown in Supplementary Fig. 3.

Membrane Morphology

Scanning electron microscopy (SEM) images of the membrane structures were obtained to characterize the effects of the different fabrication methods and the membrane-support layer configurations found in Table 1. SEM images of the DBE membrane surfaces and cross-sections are found in Fig. 4; surface and cross-section SEM images of membranes produced using SDC are found in Fig. 5. For reference, SEM images of the bare support layer are found in Supplementary Fig. 4. The presence of “sponge-like” pore structures was consistent across all membrane samples due to the use of PolarClean and GVL as solvents. In this case, the higher viscosity of this solvent mixture relative to other traditional solvents resulted in a slower rate of mixing and de-mixing during NIPS and the subsequent formation of a distinct pore structure, which is consistent with related studies involving

Fig. 3 | Partial coating window and visual representation of coating defects. **a** Partial coating window of the Psf-PolarClean-GVL dope solution on a glass plate and visual representation of **b** air entrainment and **c** dripping phenomena, highlighted with white rectangles, during single layer slot die coating process. The entire images in (b, c) are 2 mm wide.



PolarClean and GVL^{11,14,25,42}. In each cross-section image, a thin skin layer is found at the top of the membrane, which influences the selectivity of the membranes due to the presence of smaller pores in this region compared to the lower cross-sectional regions.

Below the skin layer, distinct observations were found at the membrane-support layer interface. SEM images of the cross-sections at this interface are found in Supplementary Figs. 5 and 6 for DBE and SDC membranes, respectively. Notably, SDC membranes samples that were coated onto a support layer (SDC-3 and SDC-4) exhibited spherical-shaped cavities near the membrane-support layer interface. The frequent observation of cavities at this interface indicates the occurrence of microbubbles at the interface of the substrate and Psf-PolarClean-GVL solution during the SDC process. Therefore, under the set coating parameters (flow rate of 20 mL/min, substrate velocity of 17.1 mm/s, and coating gap of 0.2 mm), the required pressure drop across the coating bead for the formation of a stable bead could not be consistently sustained. This phenomenon is attributed to a disturbance in the equilibrium with the externally imposed pressure gradient. This imbalance is primarily due to the interplay of four forces in slot die coating: viscous forces, surface tension forces, inertia forces and gravity. Concurrently, a limitation in the movement of the dynamic contact line beyond a critical speed perpendicular to its own direction leads to the emergence of sawtooth structures, as shown in Supplementary Fig. 7. The cavities led to air being trapped in the gaps where the solution did not meet the substrate^{16,18,61}. Even though membranes with a uniform surface layer were obtained, the trapped air microbubbles within the solid-liquid interface created the spherical microbubbles within the membrane matrix. This phenomenon accounted for the spherical shape of the cavities and the repeated occurrence across the interface, as illustrated in Supplementary Fig. 7. Although experimental studies have proven that the coating gap has negligible effect in viscous force dominant region in the slot die coating process, it is believed that changing the coating gap may have some impact on the formation of the microcavities observed in the produced membranes⁵⁹.

SEM images of the membrane surfaces indicate the presence of pores scattered across each sheet of generally consistent size. Based on ImageJ analysis of surface images, mean pore sizes of each membrane were approximated and are listed in Table 3. For both fabrication methods, mean pore sizes were within the reported low range of UF and slightly higher than the reported maximum pore sizes of tight NF membranes^{62,63}. Additionally, the mean pore sizes were consistent with the reported mean pore size of similar polymeric membranes prepared using PolarClean³⁰. Despite the use of different fabrication methods and the addition of the support layer, the main factors that influenced the pore development and mean pore size were constant between all samples. Namely, the dope solution composition, dope solution viscosity, and evaporation time immediately following the casting/coating step were identical, all of which dictate the exchange rate of solvent and nonsolvent and the pore formation during NIPS^{54,65}. Thus, the changes in the membrane morphology were largely found at the membrane-support layer interface, indicating that the difference in casting/coating substrate

resulted in localized morphological effects. The similarities in mean surface pore size also suggest that the membrane permeability and solute rejection would be similar between each type during filtration.

Membrane porosity

To determine the membrane void volume fraction, total porosity was measured using gas pycnometry, which are listed in Table 4. All membrane samples fabricated using DBE and all samples fabricated using SDC exhibited a mean total porosity greater than 50.0%. Additionally, total porosity was generally consistent between the two fabrication methods when analogous configurations were used. DBE-1/DBE-2 and SDC-1, both of which were prepared without a support layer, had mean total porosities of $67.7 \pm 9.1\%$ and $79.1 \pm 2.7\%$, respectively; DBE-4 and SDC-4, which were prepared on a pre-wetted support layer, had respective mean total porosities of $50.4 \pm 2.8\%$ and $54.8 \pm 1.4\%$ and DBE-3 and SDC-3 exhibited similar mean total porosities.

Total porosity measurements were validated by similar values from traditional gravimetric analysis. DBE-1/DBE-2 and SDC-1 exhibited the highest mean total porosities of $84.4 \pm 11.2\%$ and $84.3 \pm 5.4\%$, respectively, whereas the mean total porosities of membrane samples with a support layer were significantly lower. Moreover, mean total porosities of the support layer and each membrane were generally similar between the two methods. The largest discrepancy between the two methods was the mean total porosity of the support layer, which was measured to be $68.8 \pm 3.0\%$ using gas pycnometry and $31.0 \pm 5.1\%$ using the gravimetric method. This significant difference is likely due to the lower sensitivity of the latter method; namely, Silwick was unable to penetrate void spaces to the same extent as helium gas, which resulted in a lower total porosity measurement. Thus, the total porosity of the support layer aligns closer to the value obtained via gas pycnometry.

Overall, the results indicate that the support layer configuration played a dominant role in influencing membrane total porosity rather than the fabrication method. For both DBE and SDC, membranes with a support layer had a larger dry volume (V_d) than the pristine membrane, as shown in Supplementary Table 1, which is inversely proportional to total porosity and contributed to the lower total porosity values⁶⁶. Additionally, the support layer minimized lateral shrinkage of the membrane structure following the casting process; this reduction in lateral shrinkage resulted in a decrease in total porosity and has been reported in related studies^{33,49}. Furthermore, the absorbency of the polyester fabric played a role in affecting the total porosity, as the difference in wetted and dry sample weight was approximately 1.5% greater for membranes with a support layer than the pristine samples, indicating insignificant change in the amount of Silwick absorbed by the samples with a support layer.

Interfacial adhesion

The adhesion between the membrane and the support layer, whether doctor blade extruded or slot die coated, was evaluated following the ASTM

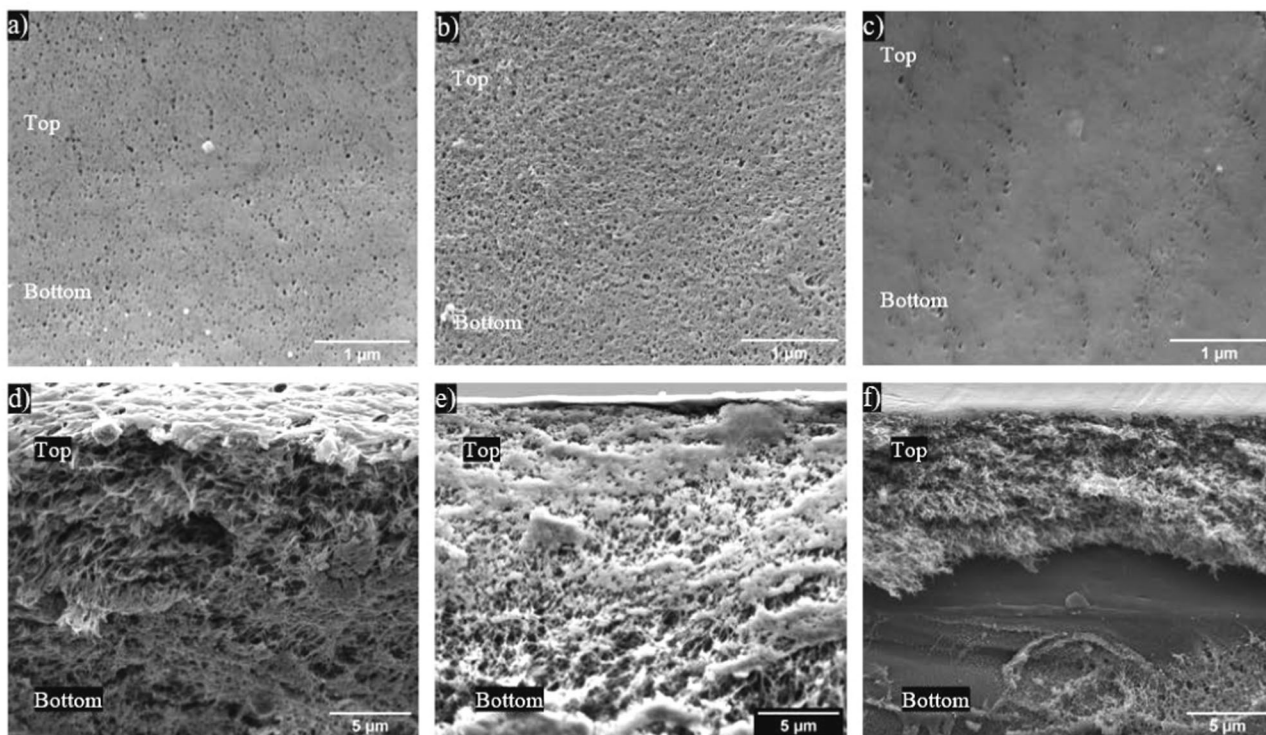


Fig. 4 | SEM images of DBE membrane samples. a DBE-1/DBE-2 surface, **b** DBE-1/DBE-2 cross-section, **c** DBE-3 surface, **d** DBE-3 cross-section, **e** DBE-4 surface, and **f** DBE-4 cross-section.

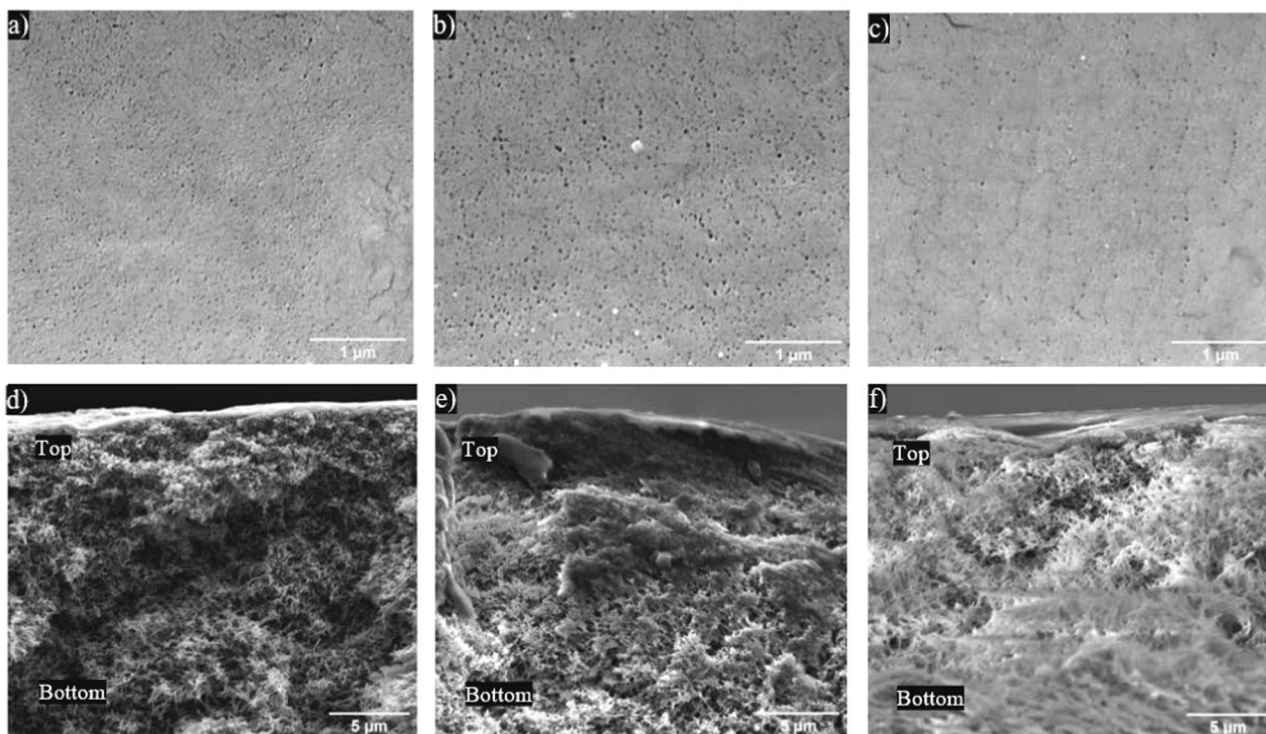


Fig. 5 | SEM images of SDC membrane samples. a SDC-1 surface, **b** SDC-1 cross-section, **c** SDC-3 surface, **d** SDC-3 cross-section, **e** SDC-4 surface, and **f** SDC-4 cross-section.

D3359 standard and the results are summarized in Fig. 6a–e. A comparative analysis of the adhesion force revealed that samples DBE-4 (Fig. 6b), SDC-3 (Fig. 6d), and SDC-4 (Fig. 6e), which correspond to the membranes cast on pre-conditioned support layers, exhibited stronger adhesion force compared to samples in Fig. 6a, c, where the membrane was coated onto the

support layer without any pre-coating process. This analysis suggests that the pre-coating process plays a crucial role in enhancing the adhesive property. The improved adhesion observed in samples that were coated onto pre-conditioned support layers can be attributed to the pre-coating process, which facilitates better interfacial interactions between the

membrane and the support layer⁹. In addition, the samples in Fig. 6d–f, which were slot die coated, exhibited enhanced adhesive force compared to the samples in Fig. 6a–c, which were doctor blade extruded. This difference is suspected to be due to different ambient conditions. DBE samples were created at a higher relative humidity and higher room temperature (RH 52% and 25 °C), while SDC samples were created at the RH of 40% and room temperature of 24 °C, as the adhesive properties can be affected by the

surrounding conditions⁶⁷. This enhanced adhesion is critical for the overall performance and durability of the membrane filters in practical applications.

Membrane filtration

Permeability and BSA rejection of the membrane samples using the dead-end filtration configuration are shown in Fig. 7a, b, respectively; mean and standard deviation values of the permeability and rejection data are compiled in Supplementary Tables 2 and 3, respectively. Overall trends in the membrane filtration characteristics were generally consistent across all samples regardless of fabrication method and support layer configuration. As seen in Fig. 7, the first 10 scatter points comprise the pre-compaction phase, whereas the final 10 scatter points were collected during BSA filtration. All membranes filtered DI water feed at permeabilities greater than 110 LMH/bar at the conclusion of the pre-compaction phase. During this phase, permeability generally decreased and approached a stabilization point as volumetric throughput increased, therefore indicating the occurrence of sufficient membrane compaction⁶⁸. The magnitude of permeability decline in the pre-compaction phase largely depended on the support layer configuration; DBE-3, DBE-4, SDC-3, and SDC-4, all of which included a support layer, exhibited a final pre-compaction permeability that was 50.6%, 51.0%, 55.8%, and 51.8% of their initial interval, respectively.

Similarly, permeability and rejection trends were relatively consistent between each sample during the BSA filtration phase. A significant decline in permeability was observed immediately due to the fouling of BSA molecules on the membrane surface. At the conclusion of filtration, DBE samples exhibited the lowest permeability with DBE-1, DBE-2, DBE-3, and DBE-4 ending at 38.9 ± 5.09 LMH/bar, 32.4 ± 2.53 LMH/bar, 33.1 ± 4.19 LMH/bar, and 32.0 ± 2.92 LMH/bar, respectively. As shown in Supplementary Fig. 8a, BSA rejection largely remained stable or declined as a function of permeability. The inclusion of the support layer in with the DBE membrane layer did not result in significant differences in membrane permeability, regardless of configuration. DBE-3 and DBE-4 exhibited similar mean BSA rejection values at $90.6\% \pm 3.86\%$ and $92.9\% \pm 3.68\%$,

Table 3 | Mean pore diameter of each membrane sample

Membrane	Mean Pore Diameter (nm)
DBE-1/DBE-2	28.4 ± 6.3
DBE-3	43.2 ± 9.1
DBE-4	40.1 ± 7.7
SDC-1	40.5 ± 10.5
SDC-3	34.6 ± 10.5
SDC-4	41.1 ± 9.45

Table 4 | Mean total porosity of the support layer and PSf-PolarClean-GVL membranes fabricated using DBE and SDC from Gas Pycnometry

Sample	Mean Total Porosity (%)
Hollytex® 3265 Nonwoven Fabric	68.8 ± 3.0
DBE-1/DBE-2	67.7 ± 9.1
DBE-3	53.0 ± 2.4
DBE-4	50.4 ± 2.8
SDC-1	79.1 ± 2.7
SDC-3	57.4 ± 2.7
SDC-4	54.8 ± 1.4

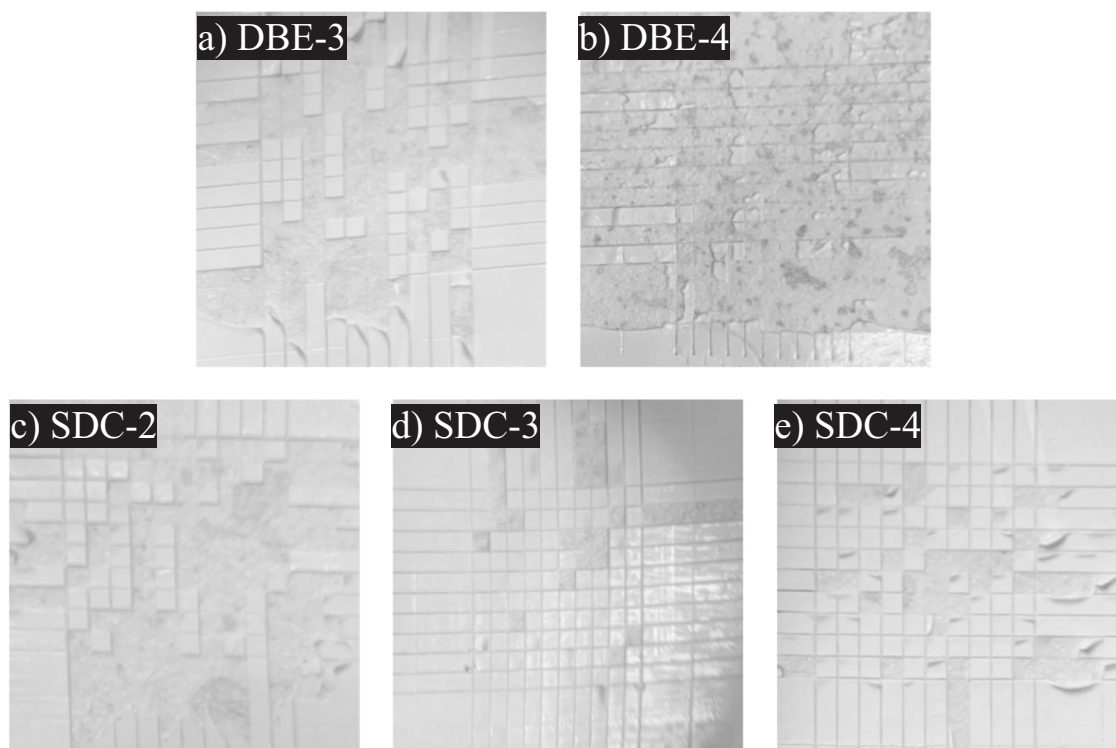


Fig. 6 | Adhesion test results for different samples. a DBE-3 with classification of 0B, **b** DBE-4 with classification of 0B, **c** SDC-2 with classification of 1B, **d** SDC-3 with classification of 3B, and **e** SDC-4 with classification of 2B.

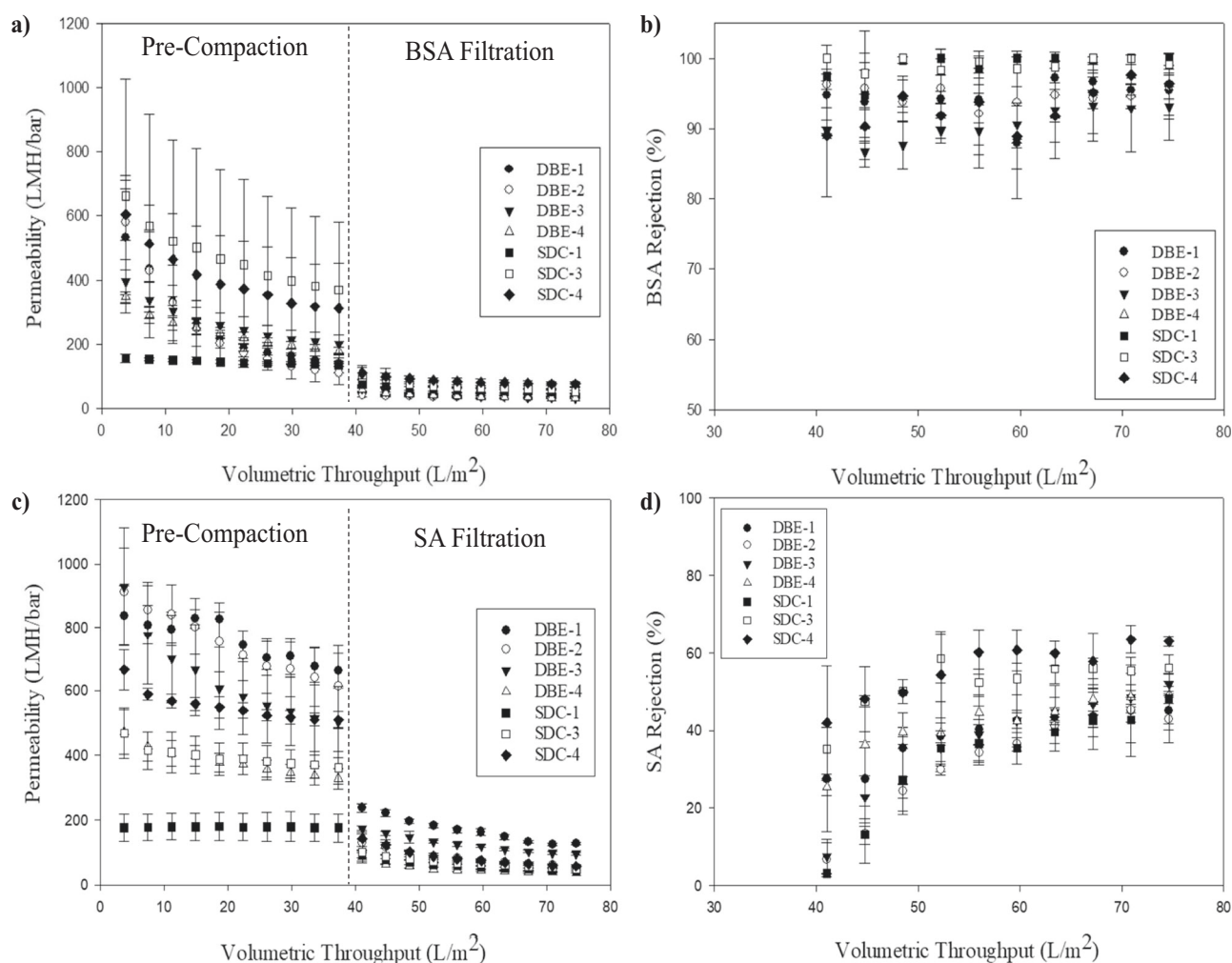


Fig. 7 | Dead-end filtration results. a BSA permeability, **b** BSA rejection, **c** SA permeability, and **d** SA rejection.

respectively, also indicating no significant differences in solute rejection. Thus, the additional steps of pre-wetting and compressing the support layer prior to coating the dope solution did not hinder the membrane performance while counteracting the dope solution penetration into the support layer.

Variability observed in membrane permeability during the pre-compaction phase was likely due to differences in thickness between the different samples. However, the similarity in performance between DBE and SDC samples during the BSA filtration phase correlates with the similarities in membrane morphology. In particular, the mean pore sizes of each sample surface were found to be within the same range, which was attributed to the dope solution composition, viscosity, and the evaporation time being constant during fabrication. Differences in the pore structure were localized to the membrane-support layer interface, where the pore structure mainly provides mechanical strength and stability for an asymmetric membrane; in contrast, the top layer provides the solute rejection through size exclusion and/or charge⁶⁹. Due to the mean pore size, high rejection, and reported properties of BSA molecules, both size exclusion and electrostatic repulsion influence the transfer mechanism. At aqueous BSA solution concentrations of 500 ppm and lower, BSA molecules tend to form aggregates and a bimodal distribution has been found in BSA molecule size with the second peak corresponding to protein aggregates of size 140–220 nm^{70,71}. Thus, the sieving of BSA aggregates accounted for a major element of the rejection process. The rejection of the remaining BSA molecules was largely attributed to

electrostatic repulsion since both PSf and BSA molecules exhibit a negative surface charge, resulting in a Donnan exclusion mechanism being present⁷¹.

Overall, SDC samples exhibited higher permeability during the BSA filtration phase as compared to DBE, as the final permeabilities of SDC-1, SDC-3 and SDC-4 were 52.1 ± 5.33 LMH/bar, 51.5 ± 14.3 LMH/bar, and 75.9 ± 7.22 LMH/bar, respectively. Despite the compression of the support layer, SDC-4 exhibited the highest mean permeability during both pre-compaction and BSA-filtration phases, though BSA rejection was relatively similar to the other SDC samples; thus, the compression of the support layer may not have resulted in significant pore size reduction of the substrate. SDC-1 and SDC-3 exhibited the highest mean BSA rejection values of $99.0 \pm 1.70\%$ and $99.2 \pm 1.31\%$, respectively. As such, the filtration results indicated that the use of SDC to produce the membranes and inclusion of a support layer did not result in a significant difference in filtration characteristics in comparison to DBE samples. Additionally, the observed presence of microbubbles at the membrane-support layer interface in SDC-3 and SDC-4 did not compromise the BSA rejection, likely due to the absence of defect formation in the selective layer at the top. Therefore, results support the ability of SDC in providing accurate scaled results of bench-scale developed membranes, and it helps narrow the gap between academic materials development and scaled fabrication.

SA, the sodium form of alginate, was selected as a secondary filtrate to model polysaccharide and other NOM filtration. Average permeability and rejection of SA as functions of volumetric throughput are found in Fig. 7c, d, respectively. Scatter point and standard deviation values for SA

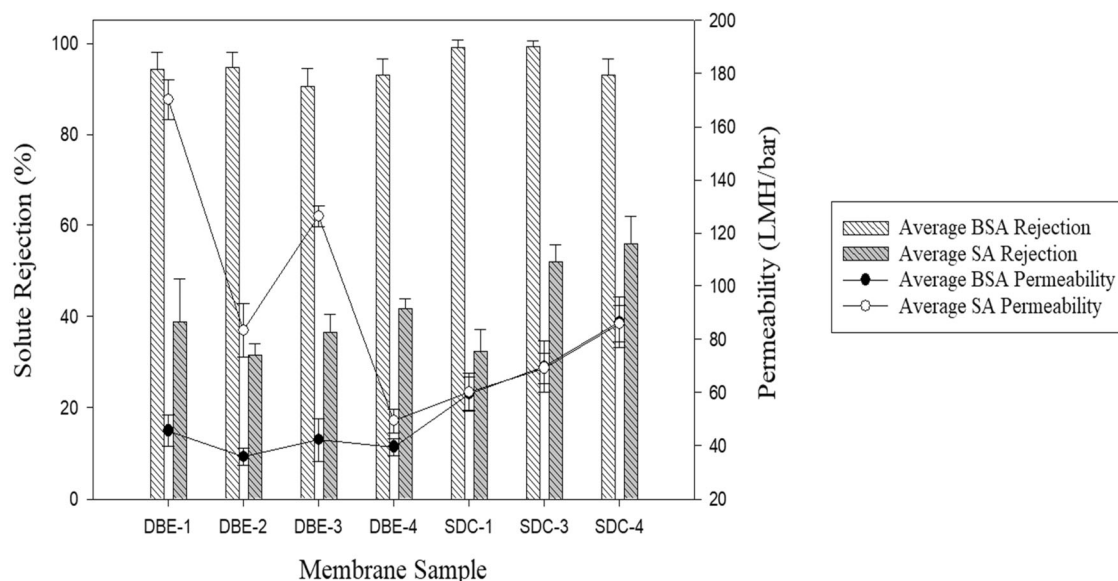


Fig. 8 | Average solute rejection and permeability of PSf-PolarClean-GVL membranes using the dead-end filtration configuration at an operating pressure of 4.14 bar and membrane cross-sectional area of 3.14 cm². Error bars represent standard deviation from the mean values.

permeability and rejection are found in Supplementary Table 4 and Supplementary Table 5, respectively. Similarly, the first 10 scatter points comprise the pre-compaction phase with DI water filtration, whereas the final 10 scatter points were from the SA filtration phase.

SA fouling was observed due to the sharp decline in permeability between the pre-compaction and SA filtration phases, validating other reports of its fouling tendency^{72,73}. Across all samples, permeability and SA rejection plateaued as volumetric throughput increased, particularly between 60 and 70 L/m². This trend is consistent with other studies on SA filtration that observed flux and rejection stabilization due to the progression of pore blocking^{74,75}. Additionally, polysaccharides exhibit strong gelation properties in water that can exacerbate fouling layer formation during filtration, which also contributed to the observed progression in fouling and SA rejection⁷⁶. In contrast to BSA filtration, Supplementary Fig. 8b indicates a clear correlation between SA rejection and permeability across all samples.

Since the interactions between alginate molecules are weak, the formation of alginate aggregates akin to BSA aggregation was likely less common; thus, the pore blocking process and observed trends in permeability and filtration were delayed in comparison to BSA filtration⁷⁴. The absence of SA aggregates and smaller particle size of SA also explain the reduction in sieving, as smaller molecules were more prone to passing through the membrane⁷⁵. Electrostatic repulsion remained a contributing factor in SA rejection due to its negative charge⁷⁷.

Correspondingly, mean SA rejection was significantly lower compared to BSA rejection. Figure 8 summarizes the mean filtration parameters of BSA and SA filtration. Although DBE membranes outperformed SDC membranes with respect to permeability, the latter group largely rejected SA more effectively. SDC-3 and SDC-4 exhibited the highest mean SA rejections of $52.0 \pm 3.8\%$ and $55.9 \pm 6.1\%$, respectively. Moreover, both samples exhibited the highest SA rejection at the onset of the SA filtration phase with SDC-3 at $35.1 \pm 6.5\%$ and SDC-4 at $41.9 \pm 14.8\%$. The mean permeability of SDC-3 and SDC-4 during SA filtration were nearly identical to the mean permeability values during BSA filtration, which may be attributed to the enhanced fouling layer formation of SA particles. The three membrane samples with a pre-wetted support layer exhibited increased mean SA rejection, as the presence of an additional dope solution layer increased the film thickness. Thus, the application of SDC and inclusion of the pre-wetted and compressed support layer improved membrane selectivity for SA filtration, indicating the possibility of improved NOM separation from feedwater.

Membrane Performance Comparison

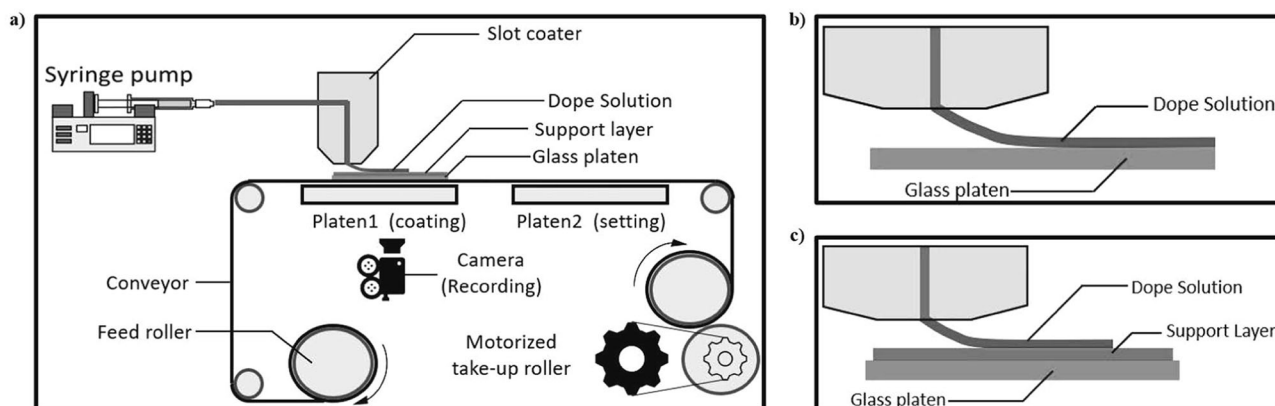
To gauge the performance characteristics of SDC-3 and SDC-4, the supported membrane samples that exhibited both high permeability and solute rejection, were compared to other loose-NF, NF, and UF membranes. Table 5 provides a comparison to other reported polymeric NF membranes prepared using PolarClean, as well as commercial UF and NF membranes. While noting that different materials and methods were used to prepare the membranes in each study, the pure water permeability (permeability measured during the final interval of the pre-compaction phase) and solute rejection values for SDC-3 and SDC-4 were found to be in a comparable range to their counterparts, validating the use of SDC as a technique to fabricate polymeric loose-NF membranes.

Discussion

The fabrication scale-up of LNF PSf flat sheet membranes with the eco-friendly solvents PolarClean and GVL was demonstrated using SDC on an R2R system. The rheological properties of the dope solution were determined to be within the reported operating limits of fluids conventionally used in SDC and were used to guide the coating parameter specifications. Membrane samples were produced at different combinations of solution flow rate and substrate speed values, which resulted in the formation of a partial coating window that visualizes the coating boundaries where air entrainment and/or dripping defects were observed. Based on the coating window and desired thickness of the membrane, a solution flow rate of 20 mL/min and substrate speed of 17.1 mm/s were selected as coating parameters to produce uniform membranes using SDC at a coating gap of 0.1 mm. A nonwoven polyester fabric support layer was incorporated as the casting/coating substrate instead of a glass plate and a pre-wetting step with dope solution was included to overcome the dope solution penetration in the support layer pores, as indicated by the Washburn equation; additionally, the pre-wetting step improved adhesion of the membrane layer to the support layer. Of the different support layer configurations that were developed and characterized, SDC-3 and SDC-4 exhibited the highest mean permeabilities of 70.5 ± 8.33 LMH/bar and 86.5 ± 9.51 LMH/bar, respectively, during BSA filtration; SDC-3 exhibited the highest mean BSA rejection of $99.2\% \pm 1.31\%$, showing that the compression of the support layer in SDC-4 did not conclusively enhance BSA rejection. The enhanced rejection of SA with mean SA rejections above 50% observed in SDC-3 and SDC-4 validated

Table 5 | Comparison of performance characteristics between NF membranes prepared using the eco-friendly solvents polarclean and/or GVL and commercial membranes

Membrane	Type	Pressure (bar)	Pure Water Permeability (LMH/bar)	Feed Solution	Rejection (%)	Source
PSf-PolarClean -GVL (SDC-3)	Flat sheet	4.14	369.0	100 ppm BSA, 100 ppm SA	99.2 (BSA) 52.0 (SA)	This study
PSf-PolarClean-GVL (SDC-4)	Flat sheet	4.14	312.3	100 ppm BSA, 100 ppm SA	93.0 (BSA) 55.9 (SA)	This study
PVDF-PolarClean	Hollow fiber	0.5	988	200 ppm polystyrene	99.9	⁹⁶
Polyester-PolarClean (M1)	Flat sheet	30	8.6 (methanol)	Oleuropein	87	⁹⁷
PVC-PolarClean (M7)	Flat sheet	6.9	3.17	2 ppm Na ₂ SO ₄	26	⁹⁸
Amicon PM30	Flat sheet	1	135	150 ppm BSA	91	⁹⁹
Dow NF 270	Flat sheet	6	16	2 ppm MgSO ₄	83	¹⁰⁰

**Fig. 9 | A simple schematic of a single-layer slot die on a R2R system. a** Overall system, close-up of the single-layer slot die lip used for **b** direct coating on a glass platen, and **c** coating on a support layer taped onto a glass platen.

this conclusion. Micro-cavities were observed at the membrane-support layer interface in SDC-3 and SDC-4, which indicated the occurrence of dripping during the deposition process; however, the isolation of the dripping-induced microbubbles to the interface resulted in no compromise in membrane performance, which indicates the microbubbles were not defects, just inconsequential irregularities. Overall, SDC samples exhibited similar properties and filtration characteristics to bench-scale DBE samples, including general pore structure, total porosity, permeability, and solute rejection. Moreover, the inclusion of the eco-friendly solvents resulted in membranes with similar performance characteristics to traditional solvent-based counterparts but with a significantly lower environmental impact and need for wastewater treatment during fabrication. Thus, the results indicate that SDC may be a promising method for translating the production of more sustainable polymeric membranes for commercial applications.

Methods

Materials

Polysulfone (PSf, average Mw 35,000 by LS, Mn 16,000 by MO, pellets) was purchased from Sigma-Aldrich (St. Louis, MO). Rhodiasolv® PolarClean was provided by Solvay. γ -valerolactone (GVL, Reagent-Plus®, 99%) was purchased from Sigma-Aldrich (Fair Lawn, NJ). Bovine serum albumin (BSA) was supplied from VWR Life Sciences (Radnor, PA). Sodium alginate (SA) was purchased from Sigma-Aldrich (Fair Lawn, NJ). Sodium sulfate anhydrous (Granular/Certified ACS) (Na₂SO₄) was supplied from Fisher Scientific (Fair Lawn, NJ). Hollytex® #3265 Nonwoven media (45" × 5 yd roll, Kavon Filter Products, Farmingdale, NJ, USA) was purchased from Talas (Brooklyn, NY, USA). Grade I deionized (DI) water at 25 °C with a resistivity of 18.2 m Ω was used to prepare filtration feed solutions.

Dope solution study

For the dope solutions, polymer and solvent weight percentages were maintained at 17% and 83%, respectively; the weight percentages were selected based on literature on UF membrane fabrication^{11,14,25}. A 3:1 ratio of PolarClean to GVL was used, as reported in Dong et al.²⁵. The dope solution was mixed using a magnetic stirring plate at 80 °C and 200 rpm for 72 h. Prior to casting, the dope solution was cooled to room temperature.

The dynamic viscosity of the dope solution was measured as first reported in Lu et al.⁴². A rheometer (AG-G2, TA instrument, DE) was used to measure the dynamic viscosity from shear rates of 0–90 s⁻¹. The dope solution surface tension was measured using a goniometer (Model 500 Advanced Goniometer/Tensiometer, ramé-hart instrument co., Succasunna, NJ) at room temperature using pendant drop method following the ASTM D7490 standard⁷⁸. A 10 mL sample of the dope solution was filled and 5 μ L of the sample was then automatically dispensed and remained at the tip of the needle to make the measurements. Ten measurements were taken and averaged. To quantify the magnitude of viscous forces acted upon the dope solution, the capillary number of the solution was calculated using Eq. 1⁷⁹:

$$Ca = \frac{\mu V}{\sigma} \quad (1)$$

where μ is the dynamic viscosity, V is the characteristic velocity or shear rate, and σ is the surface tension of the solution.

For membrane samples that included a support layer, the penetration length (L) of the dope solution in porous media in a given time was calculated through the Washburn equation, listed below as Eq. 2⁸⁰:

$$L = \sqrt{\frac{\gamma D t}{4\eta}} \quad (2)$$

where γ is surface tension of the suspension, D is average pore diameter of the porous media, t is time and η is dynamic viscosity. The result of this equation would dictate if the wetting treatment for the support layer was deemed necessary to minimize the membrane layer thinning.

Membrane fabrication

Four membrane and support layer configurations were fabricated using DBE, which are listed and visualized in Table 1. To prepare DBE-1 and DBE-2, the dope solution was cast onto a glass plate at a coating gap of 0.2 mm; during filtration experiments, DBE-1 was supported with a piece of filter paper (Qualitative Filter Paper, Grade 314, VWR, Radnor, PA, USA) and DBE-2 was supported using a piece of the support layer. To prepare DBE-3, a sheet of support layer was taped onto the glass plate and the dope solution was cast onto the support layer at a coating gap of 0.2 mm. To prepare DBE-4, a sheet of support layer was taped onto the glass plate and a preliminary layer of dope solution was cast at a coating gap of 0.05 mm as a pre-wetting treatment; subsequently, a second layer of dope solution was cast on top of the previous layer at a coating gap of 0.2 mm.

For all castings, the dope solution was spread using a doctor blade (Micrometer Adjustable Film Applicator – 250 mm, MTI Corp, Richmond, CA, USA). The plate and cast solutions were then immersed in a water nonsolvent bath to induce NIPS. An evaporation time of approximately 20 s was set in between the casting/coating and immersion steps to allow solvent at the top of the film to partially evaporate and produce a more selective skin layer⁴². Membranes were stored in DI water for at least 24 h before testing and were air-dried prior to characterization.

The fabrication of the PSf-PolarClean-GVL membrane solution was also carried out using a standard single cavity slot die, which was mounted on a roll-to-roll (R2R) system. A schematic of single-layer R2R slot die coating is presented in Fig. 9. The R2R system consisted of a PET carrier film wrapped around a feed roller, with a motorized take-up roller to regulate the substrate speed (U_w). A multiunit syringe pump was utilized to control the flow rate (Q) of the solution. To determine the coating gap (H), the offset distance between the substrate surface and the base of the slot die was measured using a dial indicator. The substrate speed was maintained at a constant value ranging from 5.4 to 40.2 mm/s throughout the process. The flow rate of the solution was set between 3.5 and 90 mL/min. The slot coater assembly, comprised of two parallel plates separated by a slot shim, was positioned above the substrate, ensuring the coating gap of 200 μm for a slot width of 200 μm (w). Samples fabricated without support layers were cast on a 20.3 cm \times 25.4 cm glass plate. Samples fabricated with a support layer were coated on a 17.8 cm \times 22.9 cm pieces of support layer, which was placed flat on a 20.3 cm \times 25.4 cm glass platen and secured with tape on all four sides. After casting the dope solution, the sample was immersed into the DI water bath for approximately 1 min. For samples that were coating on the support layer, either with or without pre-coating stage, the coated sample was first placed into the DI water bath. Then the tapes securing all four sides of the support layer were carefully removed inside the water bath. The sample remained inside the water bath for approximately 1 min before removal. Approximately 20 s of evaporation time existed at the substrate speed of 17.1 mm/s.

In the pre-coating stage, an air spray system was used to deposit a layer of the dope solution onto the surface of the support layer. The dope solution was sprayed at 5.52 bar (80 psi) for 3 min. The coating of the dope solution was confirmed visually through a noticeable color change on the surface of the support layer. This procedure was performed the fume hood, located adjacent to the R2R system. Following the pre-spray coating, the coated substrate was immediately integrated into the R2R system without any wait time. For the compression step, the support layer was manually compressed using rolling pin. The rolling pin was rolled over the surface of the support layer 20 times, which resulted in approximately 0.01 mm decrease in thickness of the support layer. The compressed support layer was immediately subjected to the following coating procedure. The four configurations are also listed and shown in Table 1.

A partial coating window for the PSf-PolarClean-GVL dope solution at a coating gap of 0.1 mm was established by identifying the stable coating region by considering the material properties of dope solution and coating parameters (e.g., substrate speed, solution flow rate) using the same methods previously reported^{14,15}. Continuous monitoring of the coating process was achieved through a camera and microscope placed beneath a transparent platen, which enabled the visualization of the dynamic wetting line during the coating process. The recorded video was subsequently analyzed to detect unstable wetting lines, which led to defects such as air entrainment or dripping. This analysis aided in identifying the substrate speed and flow rate limits, with the onset of instability determined by varying the flow rate for a given substrate speed.

Membrane characterization

The cross-sectional morphology of each membrane sample and the membrane-support layer interface were analyzed using SEM. Mean surface pore size was determined using ImageJ analysis of SEM images of the membrane surfaces at a magnification of 50,000x. Prior to imaging, samples were freeze-dried and fractured in liquid nitrogen. A 2-nm layer of platinum was applied onto the samples using a sputter-coater (Leica ACE 600 sputter-coater, Leica Microsystems, Wetzlar, Germany); for cross-section samples, a layer of colloidal graphite alcohol base was applied to the surfaces adjacent to the cross-sectional area prior to sputter-coating. SEM images were obtained using a Quanta FE/Environmental SEM.

The mean total porosity of each membrane was determined using a gas pycnometer (Accupyc 1330, Micrometrics, Norcross, GA, USA). 3 coupons with radius of 1.25 cm were inserted into the pycnometer and the helium gas feed was set to a pressure of 20 psi. Membrane volume was measured by the pycnometer based on changing the pressure of the gas by displacement in a constant volume⁸¹. Based on the sample volumes calculated by the pycnometer and the sample dimensions, porosity was calculated using Eq. 3^{66,81}:

$$\text{Total Porosity}(\%) = 1 - \frac{V_{\text{pycnometer}}}{V_{\text{geometry}}} \quad (3)$$

where $V_{\text{pycnometer}}$ represents the volume of the coupons determined by the pycnometer and V_{geometry} represents the volume of the coupons based on the dimensions. Total porosity measurements from the pycnometer were validated using the traditional gravimetric method. For each membrane, six samples were dried, and the dry weight and volume were measured. Each sample was immersed in Silwick silicon oil for 24 h and afterwards the wet weight was measured. For this method, total porosity was calculated using Eq. 4⁶⁶:

$$\text{Total Porosity}(\%) = \frac{W_w - W_0}{V_d \times \rho_s} \quad (4)$$

where W_w represents the wet sample weight in g, W_0 is the sample dry weight in g, V_d is the dry sample volume in cm^3 , and is the density of Silwick, 0.93 g/mL.

Strong adhesion of the membrane layer on the porous support layer is crucial to the mechanical integrity of the entire structure. To evaluate the adhesion force of the membranes coated using different support layer configurations, a crosscut adhesion test was performed in accordance with the ASTM D3359 standard⁸². 2 cm \times 2 cm coupons were cut from the fabricated membranes and a scratcher with 10 saws was used to create grid pattern of 100 small squares on the surface of each coupon. The scratched surface was then gently cleaned with a soft brush to remove any remaining contaminants. Scotch tape was applied to the scratched surface, ensuring good contact and complete coverage, and then carefully removed. The number of squares removed from the surface with the tape was counted to determine the adhesion classification for each sample, which ranged from 0B (>65% removal) to 5B (0% removal).

Membrane filtration

Short-term filtration experiments were conducted in a dead-end filtration cell (Amicon Stirred Cell 50 mL, UFSC05001, Millipore Sigma, Burlington, MA) at a constant pressure of 4.137 bar (60 psi). Filtration procedures were adapted from previous studies^{42,83–86}. Membrane samples were pre-compacted by filtering DI water for ten intervals. Following pre-compaction, a 100-ppm BSA solution was filtered through the membrane samples for an additional ten intervals. BSA concentration in the permeate samples was measured using a UV/Vis spectrophotometer (UV-6300PC, VWR International bvba/sprl, Leuven, Belgium) at a wavelength of 277 nm.

BSA was selected as the solute in the feed solution since it serves as a model particle for UF and NF studies; the reported surface charge and hydrodynamic size of a BSA particle provide context on the membrane filtration mechanism and pore size^{87,88}. BSA removal using nanofiltration and ultrafiltration membranes has been well-studied in literature, which provides a framework of comparison between the membranes in this study and membranes from other publications that underwent similar filtration conditions^{89–92}. Calibration curves for BSA at different concentrations are found in Supplementary Fig. 9a.

To further analyze the filtration performance of membranes with high BSA permeability and rejection, a feed solution with a 100-ppm concentration of sodium alginate (SA) was filtered through the membrane samples under the same operating conditions and experimental procedures. SA, a natural polysaccharide, is extensively studied as a natural organic matter (NOM) model foulant^{93–95}. SA concentration in the permeate samples were analyzed using the UV-Vis spectrophotometer at a wavelength of 216 nm to calculate SA rejection. Calibration curves for SA at different concentrations are found in Supplementary Fig. 9b.

Data availability

The authors confirm the data supporting the findings of the study are found within the main article and the Supporting Information. Additional data pertaining to the study may be requested from the authors.

Received: 19 September 2023; Accepted: 13 March 2024;

Published online: 28 March 2024

References

- Xu, X., Yang, Y., Liu, T. & Chu, B. Cost-effective polymer-based membranes for drinking water purification. *Giant* **10**, 100099 (2022).
- Sonawane, S., Thakur, P., Sonawane, S. H. & Bhanvase, B. A. In *Handbook of Nanomaterials for Wastewater Treatment* (eds. B. Bhanvase, S. Sonawane, V. Pawade, & A. Pandit) 537–553 (Elsevier, 2021).
- Tan, X. & Rodrigue, D. A review on porous polymeric membrane preparation. Part II: production techniques with polyethylene, polydimethylsiloxane, polypropylene, polyimide, and polytetrafluoroethylene. *Polymers* **11**, 1310 (2019).
- Robeson, L. M. In *Polymer Science: A Comprehensive Reference* (eds K. Matyjaszewski & M. Möller) 325–347 (Elsevier, 2012).
- Guo, S., Wan, Y., Chen, X. & Luo, J. Loose nanofiltration membrane custom-tailored for resource recovery. *Chem. Eng. J.* **409**, 127376 (2021).
- Shan, L. et al. Multifold enhancement of loose nanofiltration membrane performance by intercalation of surfactant assemblies. *Environ. Sci. Tech. Lett.* **5**, 668–674 (2018).
- Dong, X., Lu, D., Harris, T. A. L. & Escobar, I. C. Polymers and solvents used in membrane fabrication: a review focusing on sustainable membrane development. *Membranes* **11**, 309 (2021).
- Baig, M. I., Durmaz, E. N., Willott, J. D. & de Vos, W. M. Sustainable membrane production through polyelectrolyte complexation induced aqueous phase separation. *Adv. Funct. Mater.* **30**, 1907344 (2020).
- Garcia, J. U. et al. Mechanisms of asymmetric membrane formation in nonsolvent-induced phase separation. *ACS Macro Lett.* **9**, 1617–1624 (2020).
- Kahrs, C. & Schwellenbach, J. Membrane formation via non-solvent induced phase separation using sustainable solvents: a comparative study. *Polymer* **186**, 122071 (2020).
- Dong, X., Al-Jumaily, A. & Escobar, I. C. Investigation of the use of a bio-derived solvent for non-solvent-induced phase separation (NIPS) fabrication of polysulfone membranes. *Membranes* **8**, 23 (2018).
- Holda, A. K. & Vankelecom, I. F. Understanding and guiding the phase inversion process for synthesis of solvent resistant nanofiltration membranes. *J. Appl. Polym. Sci.* **132**, 42130 (2015).
- Chede, S., Griffiths, P., Escobar, I. C. & Harris, T. A. Does casting method matter in filtration membranes? A comparison in performance between doctor blade and slot-die extruded polymeric membranes. *J. Appl. Polym. Sci.* **135**, 45563 (2018).
- Dong, X. et al. Eco-friendly solvents and their mixture for the fabrication of polysulfone ultrafiltration membranes: an investigation of doctor blade and slot die casting methods. *J. Mem. Sci.* **614**, 118510 (2020).
- Bhamidipati, K. L., Didari, S. & Harris, T. A. L. Slot die coating of polybenzimidazole based membranes at the air engulfment limit. *J. Power Sour.* **239**, 382–392 (2013).
- Bhamidipati, K., Didari, S. & Harris, T. A. L. Experimental study on air entrainment in slot die coating of high-viscosity, shear-thinning fluids. *Chem. Eng. Sci.* **80**, 195–204 (2012).
- Kim, J. H. et al. Scalable fabrication of deoxygenated graphene oxide nanofiltration membrane by continuous slot-die coating. *J. Mem. Sci.* **612**, 118454 (2020).
- Ding, X., Liu, J. & Harris, T. A. L. A review of the operating limits in slot die coating processes. *AIChE J.* **62**, 2508–2524 (2016).
- Jin, G. L. et al. Effect of shim configuration on internal die flows for non-Newtonian coating liquids in slot coating process. *Korea-Aust. Rheol. J.* **28**, 159–164 (2016).
- Lohokare, H., Bhole, Y. & Kharul, U. J. J. Effect of support material on ultrafiltration membrane performance. *J. Appl. Poly. Sci.* **99**, 3389–3395 (2006).
- Oh, S. J., Kim, N. & Lee, Y. T. Preparation and characterization of PVDF/TiO₂ organic-inorganic composite membranes for fouling resistance improvement. *J. Mem. Sci.* **345**, 13–20 (2009).
- Sairam, M. et al. Spiral-wound polyaniline membrane modules for organic solvent nanofiltration (OSN). *J. Mem. Sci.* **349**, 123–129 (2010).
- Lohokare, H. R., Chaudhari, H. D. & Kharul, U. K. Solvent and pH-stable poly(2,5-benzimidazole) (ABPBI) based UF membranes: preparation and characterizations. *J. Mem. Sci.* **563**, 743–751 (2018).
- Gao, C., Wolff, S. & Wang, S. Eco-friendly additive manufacturing of metals: energy efficiency and life cycle analysis. *J. Manuf. Syst.* **60**, 459–472 (2021).
- Dong, X., Shannon, H. D., Parker, C., De Jesus, S. & Escobar, I. C. Comparison of two low-hazard organic solvents as individual and cosolvents for the fabrication of polysulfone membranes. *AIChE J.* **66**, e16790 (2020).
- Jordan, A., Hall, C. G. J., Thorp, L. R. & Sneddon, H. F. Replacement of less-preferred dipolar aprotic and ethereal solvents in synthetic organic chemistry with more sustainable alternatives. *Chem. Rev.* **122**, 6749–6794 (2022).
- Wang, Y. et al. Preparation and application of green sustainable solvent cyrene. *Chemistry* **5**, 2322–2346 (2023).
- Dargo, G. et al. MeSesamol, a bio-based and versatile polar aprotic solvent for organic synthesis and depolymerization. *Chem. Eng. J.* **471**, 144365 (2023).
- Russo, F., Galiano, F., Pedace, F., Aricò, F. & Figoli, A. Dimethyl isosorbide as a green solvent for sustainable ultrafiltration and microfiltration membrane preparation. *ACS Sustain. Chem. Eng.* **8**, 659–668 (2020).

30. Marino, T., Blasi, E., Tornaghi, S., Di Nicolò, E. & Figoli, A. Polyethersulfone membranes prepared with Rhodiasolv® Polarclean as water soluble green solvent. *J. Mem. Sci.* **549**, 192–204 (2018).
31. Randová, A. et al. A fundamental study of the physicochemical properties of Rhodiasolv® Polarclean: a promising alternative to common and hazardous solvents. *J. Mol. Liq.* **224**, 1163–1171 (2016).
32. Jentzer, O. & Guglieri, M. Use of esteramides as solvents, novel esteramides and process for preparing esteramides. *US Pat.*, US201402211211 (2014).
33. Xie, W. et al. First exploration on a poly (vinyl chloride) ultrafiltration membrane prepared by using the sustainable green solvent polarclean. *J. Sustain. Chem. Eng.* **8**, 91–101 (2019).
34. Hassankiadeh, N. T. et al. Microporous poly (vinylidene fluoride) hollow fiber membranes fabricated with PolarClean as water-soluble green diluent and additives. *J. Mem. Sci.* **479**, 204–212 (2015).
35. Ferlin, F. et al. Polarclean as a sustainable reaction medium for the waste minimized synthesis of heterocyclic compounds. *Front. Chem.* **6**, 659 (2019).
36. Alonso, D. M., Wettstein, S. G. & Dumesic, J. A. Gamma-valerolactone, a sustainable platform molecule derived from lignocellulosic biomass. *Green. Chem.* **15**, 584–595 (2013).
37. Dhawa, U., Tian, C., Li, W., Ackermann, L. & Cobalta-electrocatalyzed, C. -H. allylation with unactivated alkenes. *CAS Catal.* **10**, 6457–6462 (2020).
38. Nandiwale, K. Y. et al. Enhanced acid-catalyzed lignin depolymerization in a continuous reactor with stable activity. *ACS Sust. Chem.* **8**, 4096–4106 (2020).
39. Kumar, A. et al. Troubleshooting when using γ -valerolactone (GVL) in green solid-phase peptide synthesis. *Org. Process. Res.* **23**, 1096–1100 (2019).
40. Kim, J. Y., Lee, H. K., Baik, K. J. & Kim, S. C. Liquid-liquid phase separation in polysulfone/solvent/water systems. *J. Appl. Polym. Sci.* **65**, 2643–2653 (1997).
41. Yadav, P. et al. Assessment of the environmental impact of polymeric membrane production. *J. Mem. Sci.* **622**, 118987 (2021).
42. Lu, D. et al. Fabrication and evaporation time investigation of water treatment membranes using green solvents and recycled polyethylene terephthalate. *J. Appl. Polym. Sci.* **139**, e52823 (2022).
43. Xu, D., Liu, C. Y. & Craig, S. L. Divergent shear thinning and shear thickening behavior of supramolecular polymer networks in semidilute entangled polymer solutions. *Macromolecules* **44**, 2343–2353 (2011).
44. Wagner, C. E., Barbati, A. C., Engmann, J., Burbidge, A. S. & McKinley, G. H. Apparent shear thickening at low shear rates in polymer solutions can be an artifact of non-equilibration. *Appl. Rheol.* **26**, 36–40 (2016).
45. Vlachopoulos, J. & Strutt, D. In *Multilayer Flexible Packaging* 2nd edn (ed. John R. Wagner) 77–96 (William Andrew Publishing, 2016).
46. Mrokowska, M. M. & Krztoń-Maziopa, A. Viscoelastic and shear-thinning effects of aqueous exopolymer solution on disk and sphere settling. *Sci. Rep.* **9**, 7897 (2019).
47. Blake, T. D. The physics of moving wetting lines. *J. Colloid Interface Sci.* **299**, 1–13 (2006).
48. Yang, C., Wong, D. & Liu, T., Science. The effects of polymer additives on the operating windows of slot coating. *Pol. Eng. Sci.* **44**, 1970–1976 (2004).
49. Wang, S. et al. Non-woven PET fabric reinforced and enhanced the performance of ultrafiltration membranes composed of PVDF blended with PVDF-g-PEGMA for industrial applications. *Appl. Surf. Sci.* **435**, 1072–1079 (2018).
50. Yuan, Y. & Lee, T. R. Contact angle and wetting properties. in *Surface Science Techniques. Springer Series in Surface Sciences* (eds Bracco, G. & Holst, B.) Vol 51, 3–34 (Springer, 2013).
51. Blanco, J.-F., Sublet, J., Nguyen, Q. T. & Schaetzel, P. Formation and morphology studies of different polysulfones-based membranes made by wet phase inversion process. *J. Mem. Sci.* **283**, 27–37 (2006).
52. Hendrix, K., Koeckelberghs, G. & Vankelecom, I. F. J. Study of phase inversion parameters for PEEK-based nanofiltration membranes. *J. Mem. Sci.* **452**, 241–252 (2014).
53. Vogrin, N., Stropnik, Č., Musil, V. & Brumen, M. The wet phase separation: the effect of cast solution thickness on the appearance of macrovoids in the membrane forming ternary cellulose acetate/acetone/water system. *J. Mem. Sci.* **207**, 139–141 (2002).
54. Zhou, J., Ren, J., Lin, L. & Deng, M. Morphology evolution of thickness-gradient membranes prepared by wet phase-inversion process. *Sep. Purif. Tech.* **63**, 484–486 (2008).
55. Li, D., Chung, T.-S., Ren, J. & Wang, R. Thickness dependence of macrovoid evolution in wet phase-inversion asymmetric membranes. *Ind. Eng. Chem. Res.* **43**, 1553–1556 (2004).
56. Dong, X., Shannon, H. D. & Escobar, I. C. In *Green Polymer Chemistry: New Products, Processes, and Applications* 1310 ACS Symposium Series Ch. 24, 385–403 (American Chemical Society, 2018).
57. Lee, K.-Y., Liu, L.-D. & Ta-Jo, L. Minimum wet thickness in extrusion slot coating. *Chem. Eng. Sci.* **47**, 1703–1713 (1992).
58. Carvalho, M. S. & Kheshgi, H. S. Low-flow limit in slot coating: theory and experiments. *AIChE J.* **46**, 1907–1917 (2000).
59. Chang, Y.-R., Chang, H.-M., Lin, C.-F., Liu, T.-J. & Wu, P.-Y. Three minimum wet thickness regions of slot die coating. *J. Colloid Interface Sci.* **308**, 222–230 (2007).
60. Chang, H. M., Chang, Y. R., Lin, C. F. & Liu, T. J. Comparison of vertical and horizontal slot die coatings. *Poly. Eng. Sci.* **47**, 1927–1936 (2007).
61. Blake, T. D. & Ruschak, K. J. A maximum speed of wetting. *Nature* **282**, 489–491 (1979).
62. Nasir, A. M. et al. A review of the potential of conventional and advanced membrane technology in the removal of pathogens from wastewater. *Sep. Purif. Tech.* **286**, 120454 (2022).
63. Kammakakam, I. & Lai, Z. Next-generation ultrafiltration membranes: a review of material design, properties, recent progress, and challenges. *Chemosphere* **316**, 137669 (2023).
64. Genceli, E. et al. Effects of carboxylated multi-walled carbon nanotubes having different outer diameters on hollow fiber ultrafiltration membrane fabrication and characterization by electrochemical impedance spectroscopy. *Polymer Bull.* **75**, <https://doi.org/10.1007/s00289-017-2155-3> (2018).
65. Kusworo, T. D. et al. In *MATEC Web of Conferences*. 01004 (EDP Sciences).
66. Guo, Z. et al. Submicro-pore containing poly(ether sulfones)/polyvinylpyrrolidone membranes for high-temperature fuel cell applications. *J. Mater. Chem.* **3**, 8847–8854 (2015).
67. Beeldens, A., Gemert, D. V. & Aguiar, J. Aging factors affecting adhesion. in *RILEM TC 151, Adhesion technology: physical and chemical aspects*, ch. 6, 21 (2000).
68. Bilad, M. R. et al. Compaction of a polymeric membrane in ultra-low-pressure water filtration. *Polymers* **14**, 3254 (2022).
69. Mallevalle, J., Bersillon, J., Anselme, C. & Aptel, P. Membrane-filtration in drinking water treatment: A case story. in *Influence and Removal of Organics in Drinking Water* (eds Mallevalle, J. et al.) Vol. 1, 299–310 (CRC Press, 1992).
70. Madeira, P. P., Rocha, I. L. D., Rosa, M. E., Freire, M. G. & Coutinho, J. A. P. On the aggregation of bovine serum albumin. *J. Mol. Liq.* **349**, 118183 (2022).
71. Wang, L. T. et al. Separation Mechanisms and Anti-Fouling Properties of a Microporous Polyvinylidene Fluoride-Polyacrylic Acid-Graphene Oxide (PVDF-PAA-GO) Composite Membrane with Salt and Protein Solutions. *Membranes* **13**, <https://doi.org/10.3390/membranes13010040> (2022).

72. Jermann, D., Pronk, W., Meylan, S. & Boller, M. Interplay of different NOM fouling mechanisms during ultrafiltration for drinking water production. *Water Res.* **41**, 1713–1722 (2007).
73. Costa, A. R., de Pinho, M. N. & Elimelech, M. Mechanisms of colloidal natural organic matter fouling in ultrafiltration. *J. Mem. Sci.* **281**, 716–725 (2006).
74. Meng, S., Liu, H., Zhao, Q., Shen, N. & Zhang, M. Filtration performances of different polysaccharides in microfiltration process. *Processes* **7**, 897 (2019).
75. Sun, Y. et al. In *IOP Conference Series: Materials Science and Engineering*. 012031 (IOP Publishing).
76. Wang, Y. et al. Comparison of membrane fouling induced by protein, polysaccharide and humic acid under sodium and calcium ionic conditions. *Desalination* **548**, 116236 (2023).
77. Kramer, F., Shang, R., Rietveld, L. & Heijman, S. Influence of pH, multivalent counter ions, and membrane fouling on phosphate retention during ceramic nanofiltration. *Sep. Purif. Tech.* **227**, 115675 (2019).
78. ASTM, S. D7490–13 Standard test method for measurement of the surface tension of solid coatings, substrates and pigments using contact angle measurements. *B. ASTM Stand* **6**, 1–5 (2013).
79. Shi, Z., Zhang, Y., Liu, M., Hanaor, D. A. & Gan, Y. Dynamic contact angle hysteresis in liquid bridges. *Colloids Surf. A: Physicochem. Eng. Asp.* **555**, 365–371 (2018).
80. Washburn, E. The dynamics of capillary flow. *Phys. Rev.* **17**(3), 273 (1921).
81. Sreedhara, S. S. & Tata, N. R. A novel method for measurement of porosity in nanofiber mat using pycnometer in filtration. *J. Eng. Fibers Fabr.* **8**, 155892501300800408 (2013).
82. ASTM Standard D3359-02. “Standard Test Methods for Measuring Adhesion by Tape Test.” *ASTM International*, West Conshohocken, PA, <https://doi.org/10.1520/D3359-02> (2002).
83. Eke, J., Wagh, P. & Escobar, I. C. Ozonation, biofiltration and the role of membrane surface charge and hydrophobicity in removal and destruction of algal toxins at basic pH values. *Sep. Purif. Tech.* **194**, 56–63 (2018).
84. Shen, Z. et al. Fabrication of a novel antifouling polysulfone membrane with in situ embedment of mxene nanosheets. *Int. J. Env. Res. Public Health* **16**, 4659 (2019).
85. Tripathi, T., Kamaz, M., Wickramasinghe, S. R. & Sengupta, A. Designing electric field responsive ultrafiltration membranes by controlled grafting of poly (ionic liquid) brush. *Int. J. Env. Res. Public Health* **17**, 271 (2020).
86. Xu, D., Pan, G., Ge, Y. & Yang, X. Preparation of a low-protein-fouling and high-protein-retention membrane via novel pre-hydrolysis treatment of Polyacrylonitrile (PAN). *Membranes* **13**, 310 (2023).
87. Yohannes, G. et al. Thermal aggregation of bovine serum albumin studied by asymmetrical flow field-flow fractionation. *Anal. Chim. acta* **675**, 191–198 (2010).
88. Phan, H. T., Bartelt-Hunt, S., Rodenhausen, K. B., Schubert, M. & Bartz, J. C. Investigation of Bovine Serum Albumin (BSA) attachment onto Self-Assembled Monolayers (SAMs) using combinatorial Quartz Crystal Microbalance with Dissipation (QCM-D) and Spectroscopic Ellipsometry (SE). *PLoS one* **10**, e0141282 (2015).
89. Reihanian, H., Robertson, C. & Michaels, A. Mechanisms of polarization and fouling of ultrafiltration membranes by proteins. *J. Mem. Sci.* **16**, 237–258 (1983).
90. Nabe, A., Staude, E. & Belfort, G. Surface modification of polysulfone ultrafiltration membranes and fouling by BSA. *Solut. J. Mem. Sci.* **133**, 57–72 (1997).
91. Pieracci, J., Crivello, J. V. & Belfort, G. Increasing membrane permeability of UV-modified poly (ether sulfone) ultrafiltration membranes. *J. Mem. Sci.* **202**, 1–16 (2002).
92. Zhao, Z., Zheng, J., Wang, M., Zhang, H. & Han, C. C. High performance ultrafiltration membrane based on modified chitosan coating and electrospun nanofibrous PVDF scaffolds. *J. Mem. Sci.* **394**, 209–217 (2012).
93. Yusmaydiyanti, N., Desiriani, R. & Fahni, Y. Removal of total suspended solid and polysaccharide in seawater using polysulfone ultrafiltration membrane. *J. Mem. Mater.* **1**, 30–41 (2021).
94. Li, F., Deng, C., Du, C., Yang, B. & Tian, Q. Fouling mechanism and cleanability of ultrafiltration membranes modified with polydopamine-graft-PEG. *Water SA* **41**, 448–456 (2015).
95. Alsohaimi, I. H. & Hua, M. Hybrid PSf/TNT-SO₃H ultrafiltration membrane fouling by sodium alginate: effect of permeation flux on fouling resistance and desalination efficiency. *Ads. Sci. Tech.* **2022**, 1–10 (2022).
96. Jung, J. T. et al. Tailoring nonsolvent-thermally induced phase separation (N-TIPS) effect using triple spinneret to fabricate high performance PVDF hollow fiber membranes. *J. Mem. Sci.* **559**, 117–126 (2018).
97. Hardian, R., Cywar, R. M., Chen, E. Y. X. & Szekeley, G. Sustainable nanofiltration membranes based on biosourced fully recyclable polyesters and green solvents. *J. Mem. Sci. Lett.* **2**, 100016 (2022).
98. Xie, W. et al. Polydopamine/ polyethyleneimine/ MOF ternary-coated poly (vinyl chloride) nanocomposite membranes based on green solvent for shale gas wastewater treatment. *J. Membr. Sci.* **665**, 121100 (2023).
99. Salehi, E. & Madaeni, S. S. Influence of conductive surface on adsorption behavior of ultrafiltration membrane. *Appl. Surf. Sci.* **256**, 3010–3017 (2010).
100. Ağtaş, M., Ormancı-Acar, T., Keskin, B., Türken, T. & Koyuncu, İ. Nanofiltration membranes for salt and dye filtration: effect of membrane properties on performances. *Water Sci. Tech.* **83**, 2146–2159 (2021).

Acknowledgements

The authors acknowledge that this work was supported by the National Science Foundation (grant numbers 2121674 and 1922694). The authors also want to acknowledge Solvay Novecare for providing PolarClean and Arkema for supporting discussions. SEM images and sample preparation were completed using equipment at the University of Kentucky Electron Microscopy Center. The graphical abstract and select figures were created using Biorender.com. The authors also want to acknowledge Minwoo Jung and Jie Young Oh for their assistance during SDC membranes fabrication process.

Author contributions

I.C.E. and T.A.L.H. conceived and supervised the study. D.L., K.J. and J.Y.S. performed the experiments and data analyses. D.L. and K.J. wrote the paper. All authors reviewed and edited the paper. D.L. and K.J. are considered co-first authors.

Competing interests

The authors declare no competing interests.

Additional information

Supplementary information The online version contains supplementary material available at <https://doi.org/10.1038/s41545-024-00319-4>.

Correspondence and requests for materials should be addressed to Tequila A. L. Harris or Isabel C. Escobar.

Reprints and permissions information is available at <http://www.nature.com/reprints>

Publisher's note Springer Nature remains neutral with regard to jurisdictional claims in published maps and institutional affiliations.

Open Access This article is licensed under a Creative Commons Attribution 4.0 International License, which permits use, sharing, adaptation, distribution and reproduction in any medium or format, as long as you give appropriate credit to the original author(s) and the source, provide a link to the Creative Commons licence, and indicate if changes were made. The images or other third party material in this article are included in the article's Creative Commons licence, unless indicated otherwise in a credit line to the material. If material is not included in the article's Creative Commons licence and your intended use is not permitted by statutory regulation or exceeds the permitted use, you will need to obtain permission directly from the copyright holder. To view a copy of this licence, visit <http://creativecommons.org/licenses/by/4.0/>.

© The Author(s) 2024